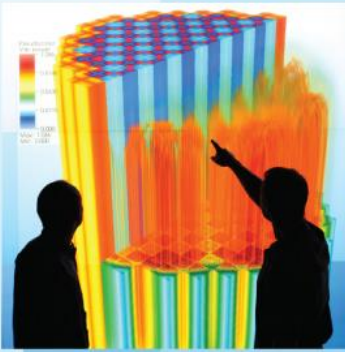




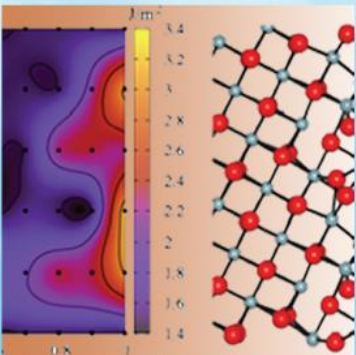
Power uprates and plant life extension



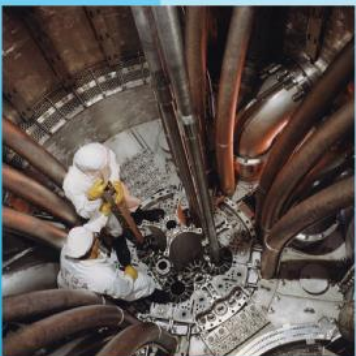
Engineering design and analysis



Science-enabling high performance computing



Fundamental science



Plant operational data

**L3:MPO.CLAD.P5.02**  
**Theoretical Investigation of**  
**Microstructure Evolution and**  
**Deformation of Zirconium**  
**under Cascade Damage**  
**Conditions**  
**A.V. Barashev, S.I. Golubov,**  
**R.E. Stoller**  
**ORNL**  
**Completed: June 22, 2012**



**THEORETICAL INVESTIGATION OF MICROSTRUCTURE EVOLUTION AND  
DEFORMATION OF ZIRCONIUM UNDER CASCADE DAMAGE CONDITIONS**

**June 2012**

**A. V. BARASHEV**  
**Oak Ridge National Laboratory**  
**University of Tennessee**

**S. I. GOLUBOV**  
**Oak Ridge National Laboratory**

**R. E. STOLLER**  
**Oak Ridge National Laboratory**

## DOCUMENT AVAILABILITY

Reports produced after January 1, 1996, are generally available free via the U.S. Department of Energy (DOE) Information Bridge.

**Web site** <http://www.osti.gov/bridge>

Reports produced before January 1, 1996, may be purchased by members of the public from the following source.

National Technical Information Service

5285 Port Royal Road

Springfield, VA 22161

**Telephone** 703-605-6000 (1-800-553-6847)

**TDD** 703-487-4639

**Fax** 703-605-6900

**E-mail** [info@ntis.gov](mailto:info@ntis.gov)

**Web site** <http://www.ntis.gov/support/ordernowabout.htm>

Reports are available to DOE employees, DOE contractors, Energy Technology Data Exchange (ETDE) representatives, and International Nuclear Information System (INIS) representatives from the following source.

Office of Scientific and Technical Information

P.O. Box 62

Oak Ridge, TN 37831

**Telephone** 865-576-8401

**Fax** 865-576-5728

**E-mail** [reports@osti.gov](mailto:reports@osti.gov)

**Web site** <http://www.osti.gov/contact.html>

This report was prepared as an account of work sponsored by an agency of the United States Government. Neither the United States Government nor any agency thereof, nor any of their employees, makes any warranty, express or implied, or assumes any legal liability or responsibility for the accuracy, completeness, or usefulness of any information, apparatus, product, or process disclosed, or represents that its use would not infringe privately owned rights. Reference herein to any specific commercial product, process, or service by trade name, trademark, manufacturer, or otherwise, does not necessarily constitute or imply its endorsement, recommendation, or favoring by the United States Government or any agency thereof. The views and opinions of authors expressed herein do not necessarily state or reflect those of the United States Government or any agency thereof.

**Materials Science and Technology Division**

**THEORETICAL INVESTIGATION OF MICROSTRUCTURE EVOLUTION AND  
DEFORMATION OF ZIRCONIUM UNDER CASCADE DAMAGE CONDITIONS**

**A. V. BARASHEV**  
**Oak Ridge National Laboratory**  
**The University of Tennessee**

**S. I. GOLUBOV**  
**Oak Ridge National Laboratory**

**R.E. STOLLER**  
**Oak Ridge National Laboratory**

**May 2012**

**Prepared by**  
**OAK RIDGE NATIONAL LABORATORY**  
**Oak Ridge, Tennessee 37831-6283**  
**managed by**  
**UT-BATTELLE, LLC**  
**for the**  
**U.S. DEPARTMENT OF ENERGY**  
**under Contract DE-AC05-00OR22725**

# CONTENTS

	page
LIST OF FIGURES .....	v
LIST OF TABLES .....	vi
ACKNOWLEDGEMENTS .....	vii
ABSTRACT .....	viii
1. INTRODUCTION .....	1
2. MODEL OF MICROSTRUCTURE EVOLUTION.....	3
2.1. Basic equations and fluxes of PDs and glissile clusters .....	3
2.2. Sessile dislocation loops .....	4
2.3. Growth strains .....	4
2.4. Dislocation velocities.....	6
2.5. Nucleation of sessile loops.....	6
3. CALCULATIONS.....	8
3.1. Fitting to experimental data .....	8
3.2. Effect of cold work.....	10
3.3. Radiation growth at high doses .....	11
3.4. Effect of vacancy loops on radiation growth .....	13
3.5. The maximum strain rate .....	18
3.6. Dislocation climb velocities .....	19
4. SUMMARY .....	20
REFERENCES .....	21
APPENDIX A. COMPUTER CODE RIMD-ZR.V1 .....	22
A1. Structure of the code .....	22
A2. Input data to the code.....	24
A3. Output files of the code.....	25
A4. Source code.....	26
A4.1. Input file: 'RIMD-ZR.dat' .....	26
A4.2. Main text: 'RIMD-ZR.f' .....	27
INTERNAL DISTRIBUTION.....	35
EXTERNAL DISTRIBUTION .....	35

## LIST OF FIGURES

1. Cartesian ( $x, y$ ) coordinate system on the basal plane, where $x$ and $y$ axes make $\alpha$ and $\pi/2+\alpha$ angles with $\mathbf{a}_1$ direction. ....	5
2. Dependence of vacancy and interstitial loop number densities on the irradiation dose .....	7
3. Comparison of the calculated growth strain and experimental measurements [17] (Figure 3b, closed symbols for iodide and open symbols for zone-refined purity).....	8
4. Growth strain for the basic set of parameters for a higher dose range .....	9
5. Calculated dose dependence of the sessile loop radii .....	9
6. Calculated dose dependence of the sessile loop sink strength. ....	10
7. Effect of cold work on the growth strain behavior .....	10
8. Dose dependence of growth strain behavior.....	11
9. Dose dependence of loop radii calculated for $\rho_d^a = 3 \times 10^{12} \text{ m}^{-2}$ .....	12
10. Dose dependence of the loop sink strengths for $\rho_d^a = 3 \times 10^{12} \text{ m}^{-2}$ .....	12
11. Enhancing radiation resistance of Zr by suppressing nucleation of c-type loops .....	13
12. Dose dependence of sessile interstitial and vacancy loop radii calculated for the case in which the initial density of $\mathbf{a}_1$ dislocations is six times higher than in the other two directions .....	15
13. Dose dependence of growth strain for the case in which the initial density of $\mathbf{a}_1$ dislocations is six times higher than in the other two directions .....	15
14. Dose dependence of growth strain for the same case as in Figure 13 designated as low dislocation density, and for the case in which all dislocation densities are increased by an order of magnitude .....	16
15. Dose dependence of loop radii for the same case as in Figure 14 .....	16
16. Dose dependence of growth strain for the case in which the initial density of $\mathbf{a}_1$ dislocations is ten time lower than in the other two $a$ directions.....	17
17. Dose dependence of loop radii for the same case as in Figure 16 .....	17
18. Growth strain behavior for different maximum concentrations of $a$ -type vacancy loops in one of the $a$ directions. The numbers 10 and 100 show the ratio of $N_v^{a_1} / N_i^{a_2}$ . Note that $c$ strains in both the cases are close to zero.....	18
19. Dislocation climb velocities at small irradiation doses for $c$ dislocations (dotted, blue –dislocation density $10^{12} \text{ m}^{-2}$ ; dash dot, wine - $10^{13}$ ; dash, blue - $10^{14}$ ) and $a$ dislocations (dot dash dot, black - $10^{12}$ ; dash dot dot, wine - $10^{13}$ ; solid, black - $10^{14}$ ) .....	19
20. Dislocation velocities as in Figure 19 but for a wider dose range .....	19

## LIST OF TABLES

	page
A1.Input parameters to the code RIMD-ZR.V1 .....	24
A2.Main output files of the code RIMD-ZR.V1 .....	25

## ACKNOWLEDGEMENTS

This research was supported by the Consortium for Advanced Simulation of Light Water Reactors (<http://www.casl.gov>), an Energy Innovation Hub (<http://www.energy.gov/hubs>) for Modeling and Simulation of Nuclear Reactors under U.S. Department of Energy Contract No. DE-AC05-00OR22725.

## ABSTRACT

This work is based on our recently-proposed reaction-diffusion model of radiation growth of Zr-based materials [1]. In Ref. [1], the equations for the strain rates in unstressed single crystal material under cascade damage conditions were derived as a function of the dislocation densities, which include a contribution from dislocation loops, and the spatial distribution of their Burgers vectors. The model takes into account the intra-cascade clustering of self-interstitial atoms and their one-dimensional diffusion; explains the growth stages, including the break-away growth of pre-annealed samples; and accounts for some striking observations, such as the negative strain in prismatic direction, and co-existence of vacancy- and interstitial-type prismatic loops. In this report, the change of dislocation density due to accumulation of sessile dislocation loops is taken into account explicitly to investigate the dose dependence of radiation growth. The dose dependence of climb rates of dislocations is calculated, which is important for the 'climb-induced glide' model of radiation creep. The results of fitting the model to available experimental data and some numerical calculations of the strain behavior of Zr for different initial dislocation structures are presented and discussed. A computer code **RIMD-ZR.V1 (Radiation Induced Microstructure and Deformation of Zr)** which has been developed is described and included as Appendix A of this report.

## 1. INTRODUCTION

The radiation growth (RG) of Zr-based materials with the hexagonal close-packed (hcp) crystal lattices is one of the damaging mechanisms which affect safe and economical operation of commercial nuclear reactors. Several theoretical models of RG have been published, including the first version by Buckley about a half of a century ago [2] (see Ref. [3] for a review). A common assumption of the models is that the primary damage is in the form of point defects (PDs), single vacancies and self-interstitial atoms (SIAs), both of which migrate three-dimensionally (3-D). This contradicts molecular dynamics (MD) simulation results on intra-cascade clustering of defects and 1-D diffusion of SIA clusters in hcp crystals [4,5]. The work by Holt *et al.* [6] is the only exception, which made an attempt to account for the defect clustering but assumed that all the clusters were immobile. The latter assumption resulted in an unreasonable requirement when fitting the model to observations; namely, the dislocation bias factor was taken to be equal to 200%, which is about two orders of magnitude larger than those derived from experimental data on swelling in [7,8] and an order of magnitude higher than those calculated using the elasticity theory [9].

Recently we proposed a reaction-diffusion model of RG [1], which is based on the Production Bias Model (PBM) [7,10-12]. The PBM provided significant success in the theory of void swelling of materials with cubic lattices. The predictions of the PBM are consistent with a broad range of experimental results, accounting for observations such as enhanced swelling near grain boundaries and void lattice formation which could not be explained by earlier models. This success is due to inclusion of (i) the cascade production and (ii) 1-D migration of SIA clusters (small interstitial-type dislocation loops) into the theory. The displacement cascades in hcp Zr are similar to those in cubic crystals; hence the PBM may provide a realistic framework for the hcp metals as well. Also, the basal-plane alignment of vacancy loops [5] and voids [13], which are observed in hcp metals irradiated at low and high temperature, respectively, is analogous to void ordering in cubic metals. Such a similarity gives additional support to the idea that, with certain modifications accounting for the features of hcp lattice, the PBM will be capable of describing RG.

In Ref. [1], the equations for the strain rates were derived as functions of dislocations densities,  $\rho_j$ , in three  $a$  and  $c$  directions:  $j = \mathbf{a}_1, \mathbf{a}_2, \mathbf{a}_3, \mathbf{c}$ . In a Cartesian coordinate system, where the  $x$  axis is along  $\mathbf{a}_1$ ,  $y$  along  $\mathbf{a}_3 - \mathbf{a}_2$  (perpendicular to  $\mathbf{a}_1$ ) and  $z$  along  $c$ , the strains,  $\varepsilon_{x,y,z}$ , evolve according to the following equations:

$$\frac{d\varepsilon_{x,y}}{d\phi} = \chi \left( \frac{1}{2} - \frac{\rho_{x,y}}{\rho} \right), \quad (1)$$

$$\frac{d\varepsilon_z}{d\phi} = -\chi \frac{\rho_z}{\rho}, \quad (2)$$

where  $\phi = G^{\text{NRT}} t$  is the irradiation dose,  $G^{\text{NRT}}$  is the NRT standard dose rate;  $\chi = (1 - \varepsilon_r) \varepsilon_i^g$ ,  $\varepsilon_r$  is the fraction of defects recombining in cascades and  $\varepsilon_i^g$  is the fraction of SIAs produced in cascades as small glissile clusters (small, perfect dislocation loops);  $\rho = \sum_j \rho_j$  is the total line density of edge dislocations and dislocation loops in all directions. By the phrase ‘dislocation or

loop in a particular direction' we mean 'dislocation or loop with the Burgers vector along this direction'. The values  $\rho_{x,y,z}$  in these equations are defined as:

$$\rho_x = \rho_{a_1} + (\rho_{a_2} + \rho_{a_3}) \cos^2(\pi/3), \quad (3)$$

$$\rho_y = (\rho_{a_2} + \rho_{a_3}) \sin^2(\pi/3), \quad (4)$$

$$\rho_z = \rho_c, \quad (5)$$

and describe the effective dislocation densities in corresponding directions:  $\rho_x + \rho_y = \rho_{a_1} + \rho_{a_2} + \rho_{a_3}$ . The total dislocation densities include contributions from sessile dislocation loops of vacancy and interstitial types:

$$\rho_j = \rho_d^j + 2\pi r_v^j N_v^j + 2\pi r_i^j N_i^j, \quad (6)$$

where  $\rho_d^j$  is the edge dislocation density, and  $r_{v,i}^j$  and  $N_{v,i}^j$  are the mean radius and number density of vacancy (subscript v) and interstitial (subscript i) loops of  $j$  orientation of the Burgers vector. These loops nucleate during irradiation and grow or shrink via interaction with mobile SIA clusters and PDs. The evolution of  $r_{v,i}^j$  and  $N_{v,i}^j$  leads to the dose dependence of dislocation structure and crystal deformation in accordance with Eqs. (1) and (2). Note that the strain rates may be rewritten for the strain tensor  $\varepsilon_{ij}$  (1=x, 2=y, 3=z) as

$$\frac{d\varepsilon_{ij}}{d\phi} = \chi \left[ \left( \frac{1}{2} - \frac{\rho_i}{\rho} \right) \delta_{ij} - \frac{1}{2} \delta_{3j} \right]. \quad (7)$$

The model proposed in Ref. [1] reproduces the RG stages observed, including the break-away growth in pre-annealed samples at high irradiation doses, and accounts for such striking observations as negative strains in prismatic directions and co-existence of vacancy- and interstitial-type prismatic loops, both of which are unexplainable in the framework of any model based on the assumption that Frenkel pair are the only form of the initial damage created by incident particles. The model gives qualitatively and quantitatively correct description for the instantaneous strain rates for a given microstructure. Accumulation of the vacancy and interstitial loops leads to evolution of the dislocation densities, hence to the dose dependence of radiation growth rates. The description of this process is the main aim of the present work.

The paper is organized as follows. In Section 2, a description of the model for the dose dependence of RG is presented. In Section 3, some calculations are presented, obtained using a computer code RIMD-ZR.V1 (**R**adiation **I**nduced **M**icrostructure and **D**eformation of **Zr**, **version 1**) developed in this work and described in Appendix A. A summary is given in Section 4.

## 2. MODEL OF MICROSTRUCTURE EVOLUTION

In accordance with our model [1], we use the following assumptions:

1. Initial microstructure consists of  $a$ - and  $c$ -type edge dislocations; densities of dislocations with the Burgers vectors along  $\mathbf{a}_1$ ,  $\mathbf{a}_2$  and  $\mathbf{a}_3$  prismatic directions,  $\rho_j$ , may be unequal;
2. Mobile PDs and SIA clusters are steadily produced in displacement cascades;
3. The PDs execute 3-D random walk, whereas SIA clusters migrate 1-D along their Burgers vectors, i.e. one of the  $\langle 11\bar{2}0 \rangle$  directions, parallel to the basal planes;
4. SIA clusters interact with dislocations of the same Burgers vector, while the much weaker interaction with other dislocations is ignored (see discussion in [1]); and
5. Repulsive interactions between various defects, the dislocation bias factor for PDs based on elastic interactions, mutual recombination of PDs, and thermal-equilibrium vacancies are ignored.

### 2.1. Basic equations and fluxes of PDs and glissile clusters

In the framework formulated above, the equations for concentrations,  $C$ , of mobile defects: single vacancies (subscript  $v$ ), single SIAs ( $i$ ) and glissile SIA clusters ( $cl$ ) are as follows (the following indexes are used:  $j = \mathbf{a}_1, \mathbf{a}_2, \mathbf{a}_3, \mathbf{c}$  and  $m = \mathbf{a}_1, \mathbf{a}_2, \mathbf{a}_3$ ):

$$\dot{C}_v = \tilde{G} - \rho D_v C_v, \quad (8)$$

$$\dot{C}_i = \tilde{G} (1 - \varepsilon_i^g) - \rho D_i C_i, \quad (9)$$

$$\dot{C}_{cl}^m = \tilde{G} \frac{\varepsilon_i^g}{3n_i^g} - k_m^2 D_{cl} C_{cl}^m, \quad (10)$$

where  $\tilde{G} = G^{\text{NRT}} (1 - \varepsilon_r)$ ;  $D_{v,i}$  are the diffusion coefficients of a single vacancy and an SIA;  $n_i^g$  is the mean number of SIAs in a cascade-produced glissile cluster;  $k_m^2$  is the sink strength for the SIA clusters migrating along  $m$  direction given by (see, e.g. [1,12,14]),

$$k_m^2 = 2 \left( \frac{\pi r_{cd} \rho_m}{2} \right)^2, \quad (11)$$

where  $r_{cd}$  is the dislocation capture radius for glissile clusters. The factor 1/3 on the right-hand side (RHS) of Eq. (10) accounts for the equality of defect production rates in the three,  $\mathbf{a}_1$ ,  $\mathbf{a}_2$  and  $\mathbf{a}_3$ , prismatic directions. The first term on the RHSs of Eqs. (8)-(10) accounts for the production of defects in cascades and the second term for their loss at dislocations, including sessile dislocation loops.

Since the mobile defects are relatively fast, the change in their concentrations happens at much higher rates than the changes in the sessile loop population. For this reason, the steady-state approximation for the defects fluxes is appropriate when analyzing the evolution of the microstructure. The steady-state fluxes of mobile species,  $DC^{\text{ss}}$ , can be found by setting the time derivatives in Eqs. (8)-(10) to zero:

$$D_v C_v^{ss} = \frac{\tilde{G}}{\rho}, \quad (12)$$

$$D_i C_i^{ss} = (1 - \varepsilon_i^g) \frac{\tilde{G}}{\rho}, \quad (13)$$

$$D_{cl} C_{cl}^{m,ss} = \frac{1}{3n_i^g} \frac{\tilde{G} \varepsilon_i^g}{k_m^2}. \quad (14)$$

The steady state is assumed below, but the superscript ‘ss’ is omitted to simplify notation.

## 2.2. Sessile dislocation loops

A detailed description of the population of sessile vacancy- and interstitial-type dislocation loops can be obtained from the master equations in terms of the corresponding size-distribution functions. Then, generally a large number of equations is considered, one for each cluster size, which would require employing some grouping procedure to reduce the number of equations such as that proposed in Ref. [15]. To avoid associated complications, we use the mean-size approximation, where the mean values of  $r_{v,i}^j$  for the sessile vacancy and interstitial loops are found via the relationship between the loop number density,  $N$ , the total number of defects in the loops of any particular type,  $S$ , and the loop Burgers vector  $\mathbf{b}$ :

$$S = \pi r^2 b N. \quad (15)$$

The values  $N$  and  $S$  are found from ‘exact’ equations, which do not require knowledge of the size-distribution function. Loop nucleation and the corresponding equations for the number density of sessile loops are considered below in Section 2.5. The total numbers of defects (per atomic site) in the loops change with time according to the following equations.

$$\dot{S}_v^m = 2\pi r_v^m N_v^m (D_v C_v - D_i C_i) - k_{vm}^2 n_i^g D_{cl} C_{cl}^m, \quad (16)$$

$$\dot{S}_i^m = -2\pi r_i^m N_i^m (D_v C_v - D_i C_i) + k_{im}^2 n_i^g D_{cl} C_{cl}^m, \quad (17)$$

$$\dot{S}_v^c = 2\pi r_v^c N_v^c (D_v C_v - D_i C_i), \quad (18)$$

where  $N_{v,i}^m$  are the number densities of vacancy and interstitial loops in  $m$  direction; and the total sink strengths of sessile dislocation loops for glissile clusters are given by

$$k_{vm}^2 = 2\pi^2 r_{cvl} r_v^m N_v^m \left( \frac{\pi r_{cd}}{2} \rho_d^m + \pi^2 r_{cvl} r_v^m N_v^m + \pi^2 r_{cil} r_i^m N_i^m \right), \quad (19)$$

$$k_{im}^2 = 2\pi^2 r_{cil} r_i^m N_i^m \left( \frac{\pi r_{cd}}{2} \rho_d^m + \pi^2 r_{cvl} r_v^m N_v^m + \pi^2 r_{cil} r_i^m N_i^m \right), \quad (20)$$

where  $r_{cvl}$  and  $r_{cil}$  are the capture radii of sessile vacancy- and interstitial-type prismatic loops for glissile SIA clusters. These equations represent generalized versions of Eq. **Error! Reference source not found.** [12,14].

## 2.3. Growth strains

To formulate equations for the strain rates in prismatic ( $m = \mathbf{a}_1, \mathbf{a}_2, \mathbf{a}_3$ ) and basal ( $\mathbf{c}$ ) directions, let us first consider the change of the quantities  $E$ : the net numbers of SIAs (i.e. the number of SIAs

minus number of vacancies) accumulated by dislocations and loops in different directions. As follows from Eqs. (8)-(10), these are equal to the sums of contributions from the glissile clusters (for prismatic directions), and PDs captured by dislocations and sessile loops (for all directions):

$$\dot{E}_m = \frac{1}{3} \chi G - \rho_m (D_v C_v - D_i C_i), \quad (21)$$

$$\dot{E}_c = -\rho_c (D_v C_v - D_i C_i), \quad (22)$$

The strain in prismatic directions is described by a two-dimensional tensor,  $\varepsilon_{ik}$ , which can be found using Eq. (21). In a Cartesian coordinate system with the  $x$ -axis lying in the basal plane and making angle  $\alpha$  with  $\mathbf{a}_1$  direction (see Figure 1):

$$\varepsilon_x = E_{a_1} \cos^2 \alpha + E_{a_2} \cos^2 (\alpha - \pi/3) + E_{a_3} \cos^2 (\alpha + \pi/3). \quad (23)$$

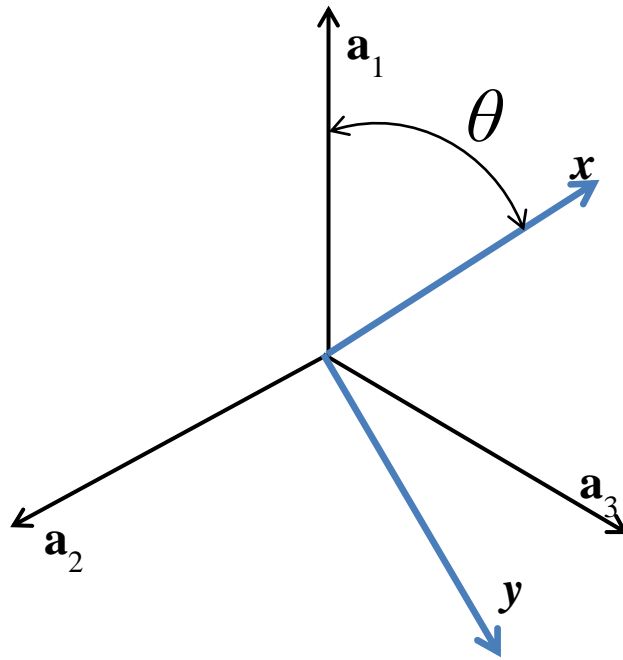


**Figure 1.** Cartesian  $(x, y)$  coordinate system on the basal plane, where  $x$  and  $y$  axes make  $\alpha$  and  $\pi/2+\alpha$  angles with  $\mathbf{a}_1$  direction.

It can readily be shown that the strain tensor  $\varepsilon_{ik}$  is diagonal in a Cartesian coordinate system where the  $x$  and  $y$  axes make  $\alpha_0$  and  $\pi/2+\alpha_0$  angles with  $\mathbf{a}_1$  (see figure 1), and  $z$  is along  $\mathbf{c}$ , and if

$$\alpha_0 = \frac{1}{2} \operatorname{arctg} \left[ \frac{\sqrt{3}(E_{a_2} - E_{a_3})}{2E_{a_1} - E_{a_2} - E_{a_3}} \right] \pm \frac{\pi}{2} k, \quad (24)$$

where  $k$  is an integer. In such a system, the strain field is described by an ellipsoid with  $x$  and  $y$  the principal axes [16], while the strain along any particular direction  $\mathbf{l}$  is given by a simple sum:

$$\varepsilon_{\mathbf{l}} = \varepsilon_x \cos^2 (\mathbf{l}, x) + \varepsilon_y \cos^2 (\mathbf{l}, y) + \varepsilon_z \cos^2 (\mathbf{l}, z), \quad (25)$$

where,  $(\mathbf{l}, x)$  denotes the angle between the two directions in the brackets. In other coordinate systems, e.g. when  $\alpha \neq \alpha_0$ , the difference in the quantities defined by Eqs. (25) and (23) is given

by  $\frac{\sqrt{3}}{4}(\varepsilon_{a_3} - \varepsilon_{a_2})\sin(2\alpha)$ . Hence, the strains along principal axes of the coordinate system with the  $x$  axis along  $\mathbf{a}_1$  direction, i.e. for  $\alpha_0 = 0$ , are always correct.

As we argue in Sections 3.3 and 3.4, at relatively high doses the dislocation structure tends to be isotropic in prismatic directions, hence one can assume that  $\alpha_0 = 0$ . At low doses, such an assumption is, strictly speaking, incorrect, and the exact Eq. (23) should be used. However, since with  $\alpha_0 = 0$ , the strains along principal axes are correct, and their interpolation by the simpler Eq. (25) may be used as a first approximation to the exact values.

## 2.4. Dislocation velocities

The dislocation climb rates, i.e. velocities  $V_j$ , are in general different for different directions and can be calculated using the relationship

$$E_j = \rho_j V_j b_j, \quad (26)$$

where  $\rho_j$  is the total dislocation density including contribution from dislocation loops with the Burgers vector along  $j$  direction. These are needed for calculating the creep rate using the ‘climb-induced glide’ models. In this case, the model proposed for the description of RG provides a link to a description of creep, at least for this particular mechanism.

## 2.5. Nucleation of sessile loops

In contrast to the loop growth/shrinkage during irradiation/ageing, which has been studied extensively, their nucleation is not well understood. There is no fundamental information on the nucleation mechanisms of sessile dislocation loops in hcp metals, including Zr. For this reason, here we use a simple description, which satisfies the following four conditions:

1. Interstitial and vacancy prismatic loops form from the very beginning of irradiation until reaching maximum number densities of  $N_{v,i}^{a,\max} \approx 10^{22} \text{ m}^{-3}$ ;
2. Basal vacancy loops start nucleating after some critical dose,  $\phi_{v0}^c \approx 3 \text{ dpa}$ , until reaching a number density  $N_v^{c,\max} \approx 10^{21} \text{ m}^{-3}$ ;
3. The nucleation process ceases at some dose less than several tens of dpa. This assumption is based on our experience in the theory of nucleation in metallic systems;
4. Loop nuclei consumed only a negligible fraction of irradiation-produced defects. This is based on our estimates using experimental data on loop radii and densities; and
5. Nucleation of sessile loops takes place when the net flux of corresponding defects, SIAs for interstitial loops and vacancies for vacancy loops, is positive (corresponding  $\dot{S}$  in Eqs. (16) and (17) is positive).

To describe evolution of the number densities, we use the following functions

$$N_{v,i}^m = \begin{cases} N_{v,i}^{m,\max} \phi / \phi_{v,i}^{\max}, & \phi \leq \phi_{v,i}^{\max} \\ N_{v,i}^{m,\max}, & \phi > \phi_{v,i}^{\max} \end{cases}, \quad \dot{S}_{v,i}^m > 0, \quad (27)$$

$$N_v^c = \begin{cases} 0, & \phi < \phi_{v0}^c \\ N_v^{c,\max} \frac{\exp[A(\phi - \phi_{v0}^c)/\Delta] - 1}{\exp(A) - 1}, & (\Delta + \phi_{v0}^c) > \phi \geq \phi_{v0}^c \\ N_v^{c,\max}, & \phi \geq (\Delta + \phi_{v0}^c). \end{cases} \quad (28)$$

In these equations,  $A$  is a dimensionless parameter, while  $\phi_{v,i}^{\max}$  and  $\Delta$  characterize doses at the end of the nucleation stages for sessile vacancy- and interstitial-type prismatic loops, and sessile vacancy basal loops, respectively. This is for the case of continuous nucleation, otherwise the nucleation stops when the maximum number density:  $N_{v,i}^{m,\max}$  and  $N_v^{c,\max}$  is reached.

Assumption 4 above enables the fractions of irradiation-produced defects which create loop nuclei in the evolutionary equations of the previous Sections to be neglected. This requires determining explicitly finite loop nuclei radii; otherwise the loops would not grow, since their growth rate is proportional to their radius. We used the condition  $S_{i,v}^m = S_0$ , where  $S_0$  is equal to some small value  $\sim 10^{-10}$ .

Figure 2 shows the loop number density evolution for  $N_v^{a,\max} = N_i^{a,\max} \approx 10^{22} \text{ m}^{-3}$ ,  $\phi_v^{\max} = \phi_i^{\max} = 3.84 \text{ dpa}$ ,  $\phi_{v0}^c \approx 3 \text{ dpa}$ ,  $N_v^{c,\max} \approx 10^{21} \text{ m}^{-3}$  and  $\Delta = 10 \text{ dpa}$ . The total number density of prismatic loops is defined as the sum  $N_{v,i}^{a,\max} = N_{v,i}^{a1,\max} + N_{v,i}^{a2,\max} + N_{v,i}^{a3,\max}$ .) These functions are close to experimental data in Ref. [17] and were used in the basic parameter set for the calculations presented in the following section. The total basic set of parameters is given in A.4.1.

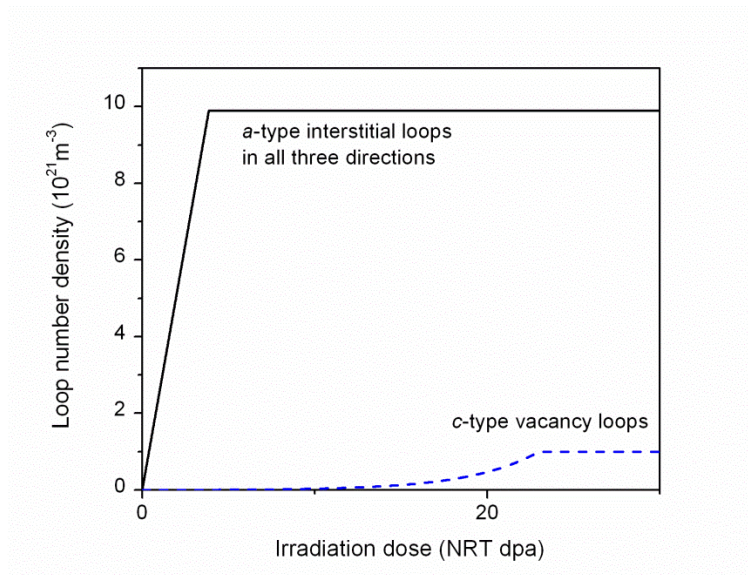


**Figure 2.** Dependence of vacancy and interstitial loop number densities on the irradiation dose.

### 3. CALCULATIONS

A computer code RIMD-ZR.V1 (Radiation Induced Microstructure and Deformation of Zr, Version 1) implementing the scheme described above has been developed, see Appendix A. It was used to study evolution of the microstructure of a sample during neutron irradiation. Selected results are presented below.

#### 3.1. Fitting to experimental data

Figure 3 shows the results of using experimental data from Ref. [17] to adjust model parameters. The NRT standard dose was calculated from the fluence, assuming that  $10^{25} \text{ n/m}^2 = 1 \text{ dpa}$ . The number densities of dislocation loops shown in Figure 2 have been used. The best fit parameters are:  $\varepsilon_r = 0.9$  and  $\varepsilon_1^g = 0.2$ ; while the interaction radii of the SIA clusters with dislocations and loops were taken to be  $r_{cd} = r_{cvi} = r_{cil} = 0.6 \text{ nm}$ . The value of  $\chi = 0.02$  was found to be the same as that extracted from experiments on fcc Cu in [7]. These parameters were used as the basic set in the following calculations and a list of the parameters is given in section A.4.1 in the input file to the code.

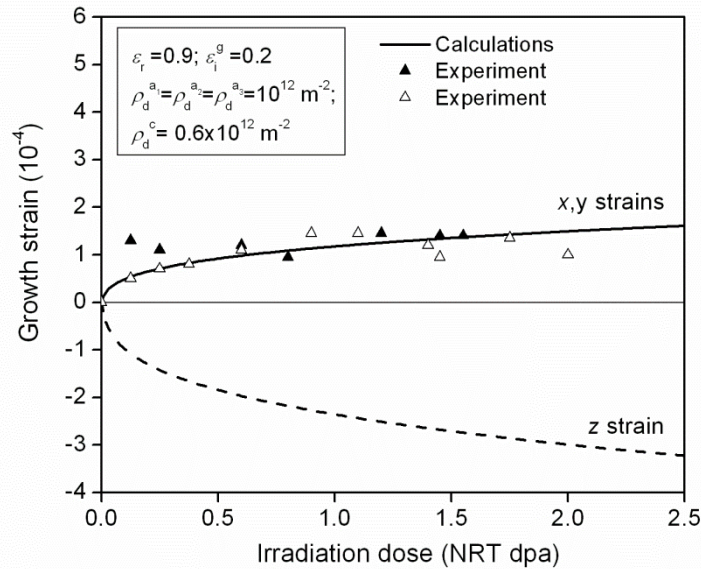


**Figure 3.** Comparison of the calculated growth strain and experimental measurements [17] (Figure 3b, closed symbols for iodide and open symbols for zone-refined purity).

The results in Figure 3 were obtained for an isotropic distribution of prismatic dislocations. The  $c$ -strain in this case is two times larger than that for any of the  $a$ -directions. This is not always the case in experiments, as shown in Figure 4a [17], where the  $c$ -strain is even smaller than that in  $a$ -direction. The main reasons for this observation may be a non-isotropic distribution of prismatic dislocations. The latter effect is considered in the following sections.

The strain behavior calculated for a wider dose range, which includes the break-away stage, is presented in Figure 4 using the same parameters as were used for Figure 3. These results

demonstrate that the function chosen to describe nucleation of vacancy *c*-type loops gives strain values during the break-away stage which are similar to those observed experimentally [17].

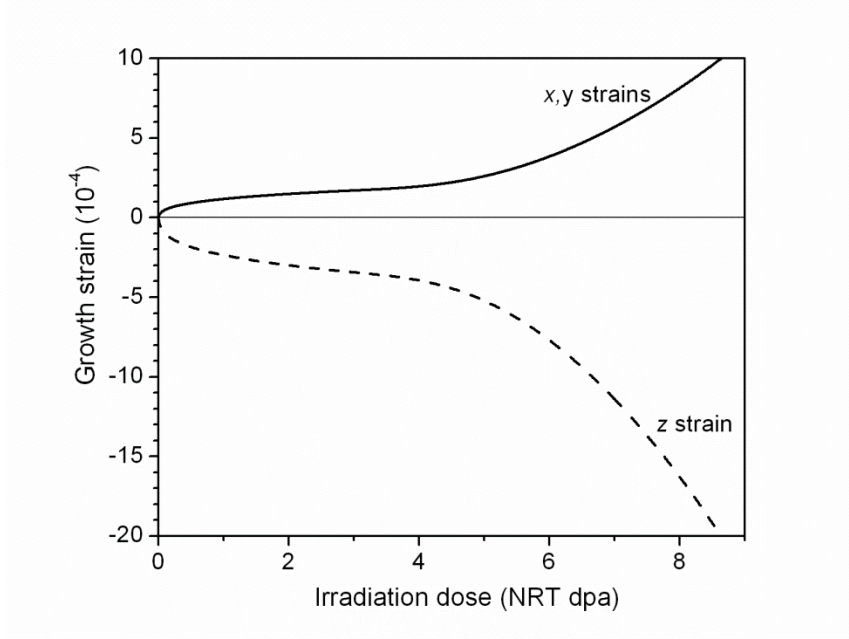


**Figure 4.** Growth strain for the basic set of parameters for a higher dose range.

The experimentally observed values of ~10 nm for the radii of interstitial *a*-type loops and ~300 nm for the vacancy *c*-type loops are also reproduced well by this parameter set, as shown in Figure 5.

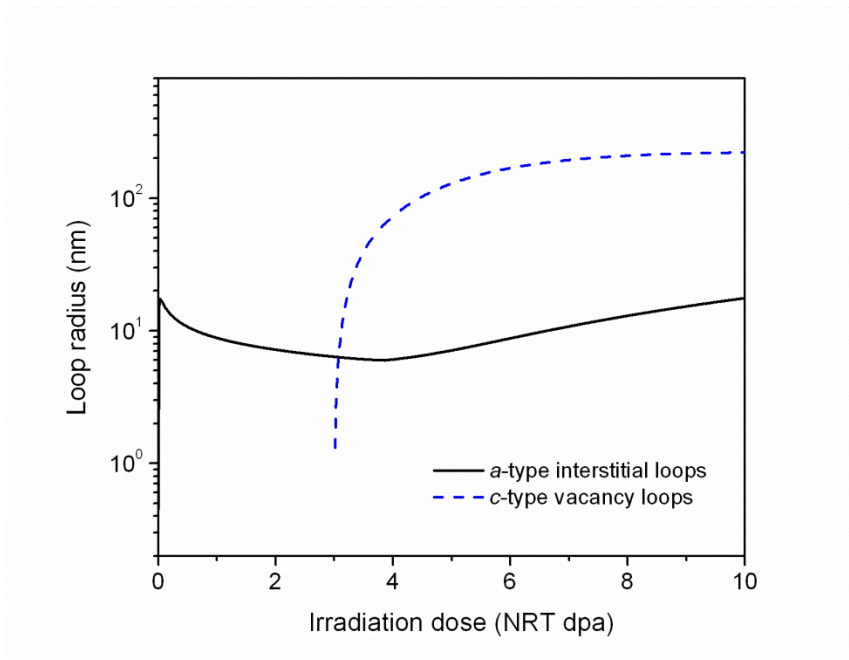


**Figure 5.** Calculated dose dependence of the sessile loop radii.

Note that a small decrease in the mean size of *a*-loops in the intermediated dose range may be an artificial effect due to the mean-size approximation used. However, this is not a problem since the more important integral values, which affect strain behavior, behave well, e.g. the loop sink strength increases steadily with increasing irradiation dose, as shown in Figure 6.

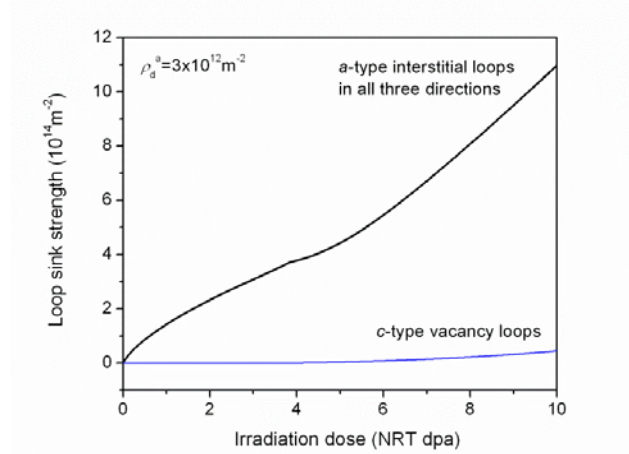


**Figure 6.** Calculated dose dependence of the sessile loop sink strength.

### 3.2. Effect of cold work

The effect of cold-work on the strain behavior is demonstrated in Figure 7. An increase of all dislocation densities in the basic parameter set by an order of magnitude increases the strains (dashed line, compare with solid line for the basic parameter set), but the tendency toward saturation is maintained. Another tenfold (or higher) increase of the densities gives steep straight (dotted) line with the slope  $\sim 1.7 \times 10^{-3}/\text{dpa}$ , as indicated in the figure. This is in a good agreement with the maximum of  $\sim 10^{-3} \text{ dpa}^{-1}$  observed for swaged Zr [17]. The value of  $10^{-3}/\text{dpa}$  is reproduced by our calculations, when the ratio of *a* to *c* dislocation densities is two times higher:  $\rho_d^a / \rho_d^c = 10$  (dash-dotted line).

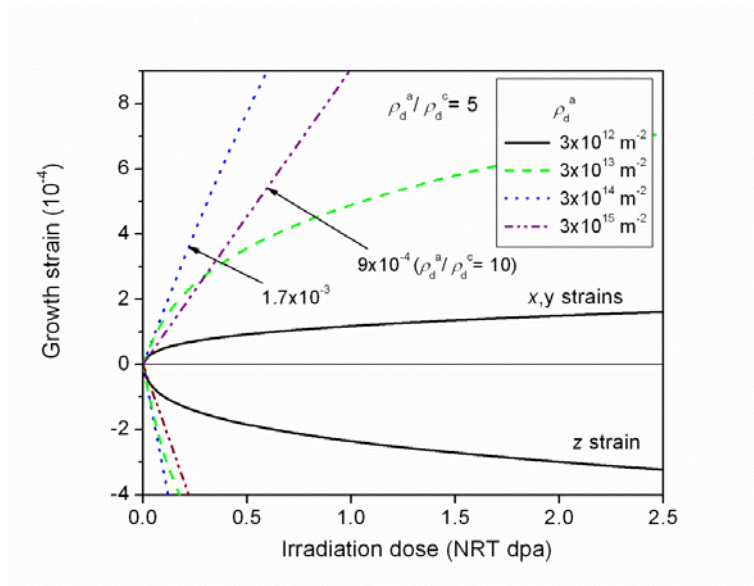


**Figure 7.** Effect of cold work on the growth strain behavior.

### 3.3. Radiation growth at high doses

Figure 8 shows the dose dependence of growth strain at high irradiation doses of up to 100 dpa. Two calculations, for low and high dislocation densities, are presented. These show remarkable qualitative, as well as quantitative, differences in the strain behavior in the dose range up to 2.5 dpa in Figure 7 (cf. solid and dotted lines). The difference between the predicted strains diminishes at high doses. This is because sessile loop nucleation and growth causes their sink strength to become significantly higher than that of pre-existing dislocations very early during irradiation. irradiation (see Figure 9 shows the dose dependence of the loop radii and Figure 10 shows the calculated loop sink strength. The sink strength of these loops then govern the strain behavior, independent of initial dislocation density. In the high-dose range, the calculations presented in Figure 8 depend mainly on the ratio of maximum number densities for sessile *a*-type interstitial and *c*-type vacancy loops,  $N_i^{a,max} / N_v^{c,max}$ . As indicated in the figure, a value of 10 was used in these calculations.

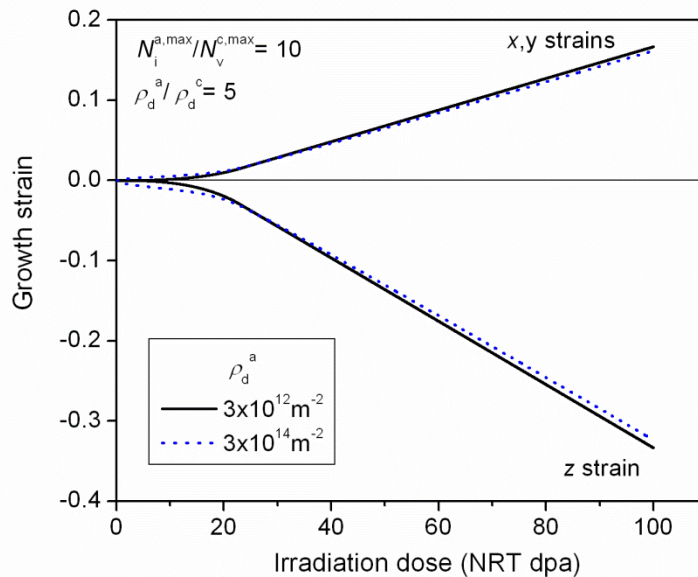


**Figure 8.** Dose dependence of growth strain behavior.

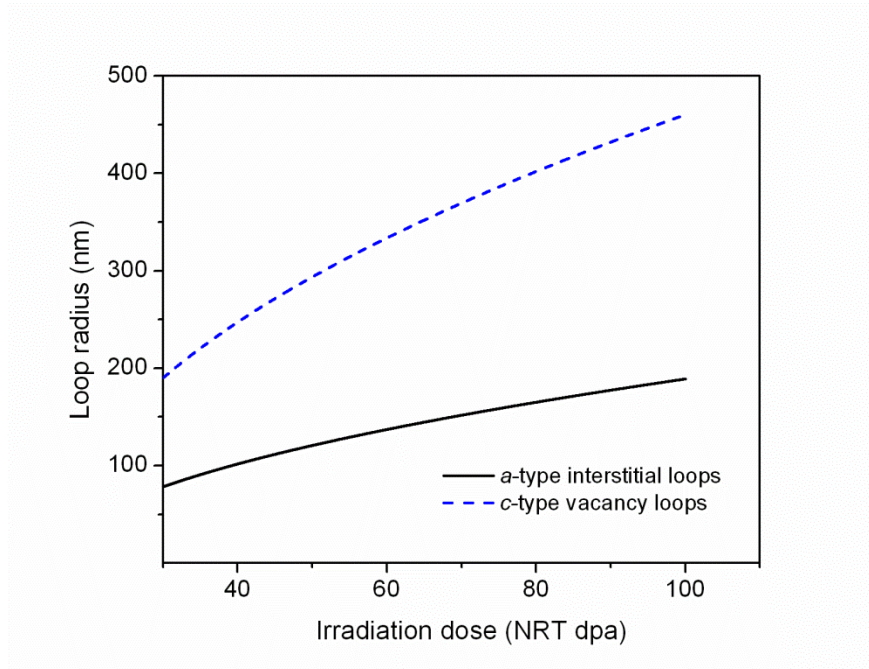


**Figure 9.** Dose dependence of loop radii calculated for  $\rho_d^a = 3 \times 10^{12} \text{ m}^{-2}$ .

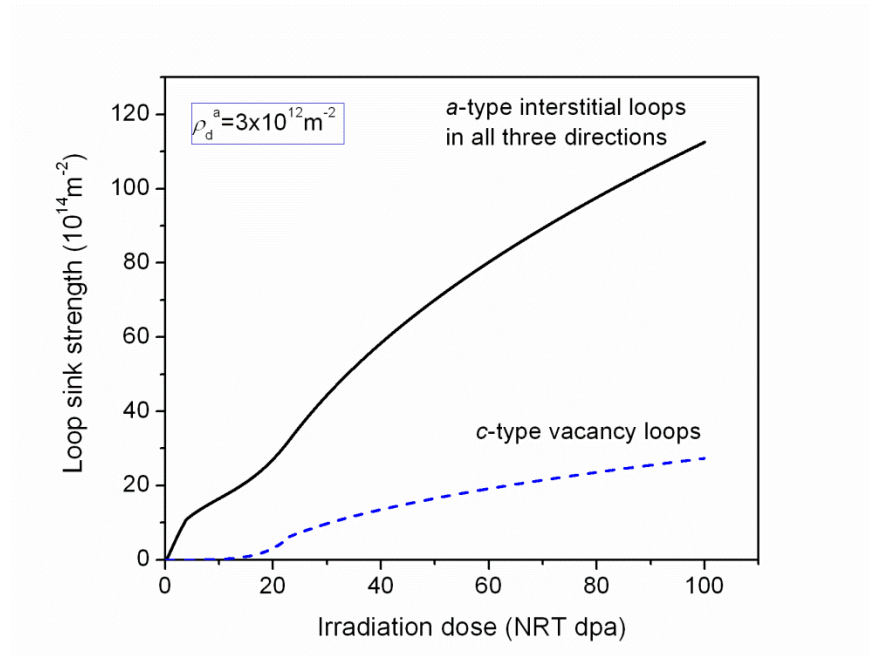


**Figure 10.** Dose dependence of the sink strength of sessile loops for the basic parameter set and  $\rho_d^a = 3 \times 10^{12} \text{ m}^{-2}$ .

Figure 11 shows the decrease of the growth strain with an increasing ratio of *a*- to *c*-loop densities. By suppressing the nucleation of *c*-type loops, one can decrease the strains and thereby enhance the radiation resistance of Zr.

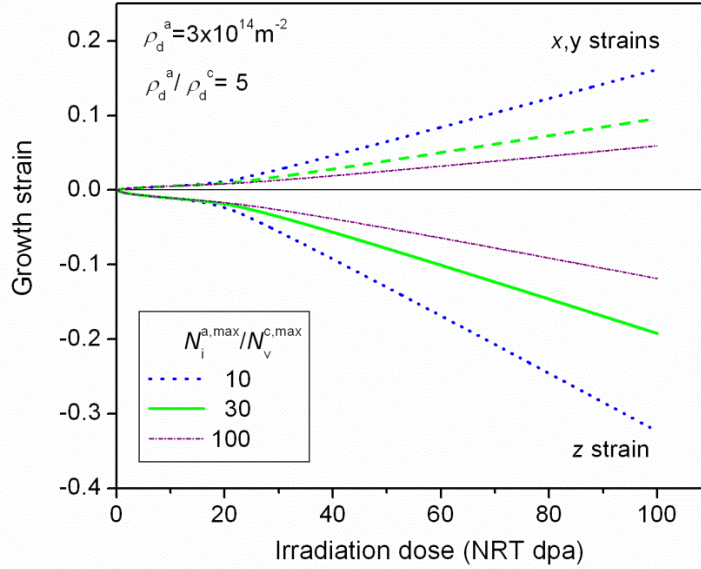


**Figure 11.** Enhancing radiation resistance of Zr by suppressing nucleation of *c*-type vacancy loops leading to a decreased ratio of *a*- to *c*-loop densities.

The behavior at very high irradiation dose, when dislocation loops govern the evolution, and vacancies are mainly collected in *c*-type vacancy loops and SIAs in *a*-type interstitial loops, can be obtained from Eqs. (1) and (2) using the conservation law  $\pi(r_i^a)^2 N_i^{a,max} b = \pi(r_v^c)^2 N_v^{c,max} b$  and Eq. (6):

$$\frac{d\varepsilon_z}{d\phi} = -2 \frac{d\varepsilon_x}{d\phi} = -2 \frac{d\varepsilon_y}{d\phi} = -\chi \frac{1}{1 + \sqrt{N_i^{a,max} / N_v^{c,max}}}. \quad (29)$$

According to this equation, the strain rates at high irradiation doses and a relatively low number density of *c*-type vacancy loops:  $N_i^{a,max} \gg N_v^{c,max}$ , must be proportional to the square root of the ratio of their number densities:

$$\left( \frac{d\varepsilon_z}{d\phi} \right)_{\phi \rightarrow \infty} \approx -\chi \sqrt{N_v^{c,max} / N_i^{a,max}}. \quad (30)$$

### 3.4. Effect of vacancy loops on radiation growth

It can readily be shown using Eqs. (16)-(17) and (12)-(14) that, if the total dislocation density in one direction (e.g.  $\mathbf{a}_1$ ) is higher than in the other two directions, then vacancy loops grow in this direction, while interstitial loops grow in the other two directions. If the dislocation densities in  $\mathbf{a}_2$  and  $\mathbf{a}_3$  directions are equal, the evolution of the dislocation line densities in  $\mathbf{a}_1$ ,  $\mathbf{a}_2$  and  $\mathbf{a}_3$  directions are described by the following equations:

$$\frac{d\rho_{a_1}}{d\phi} = \chi \frac{2\pi N_v^{a_1}}{3b} \left[ \frac{2(\rho_{a_1} - \rho_{a_2}) - \rho_c}{\rho_{a_1}\rho} \right], \quad (31)$$

$$\frac{d\rho_{a_2}}{d\phi} \equiv \frac{d\rho_{a_3}}{d\phi} = \chi \frac{2\pi N_i^{a_2}}{3b} \left[ \frac{(\rho_{a_1} - \rho_{a_2}) + \rho_c}{\rho_{a_2}\rho} \right]. \quad (32)$$

The vacancy loops can grow, when the RHS of Eq. (31) is positive, meaning

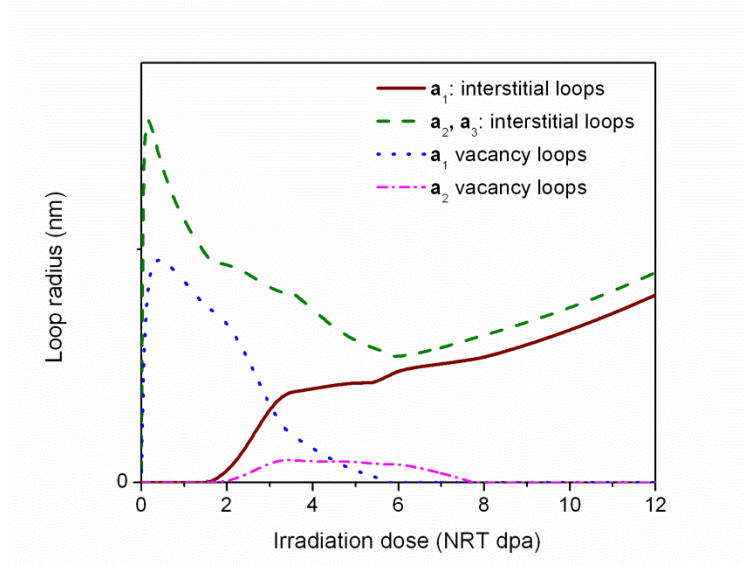
$$2(\rho_{a_1} - \rho_{a_2}) > \rho_c. \quad (33)$$

This may be true in the beginning of irradiation, when only preexisting dislocations are present. However, if interstitial  $a$ -loop line density accumulates faster than that of vacancy  $a$ -loops, the LHS of Equation (31) may become negative, and the vacancy loops will start dissolving. The line density of interstitial loops increases faster if the ratio of Eqs. (31) and (32) is smaller than unity:

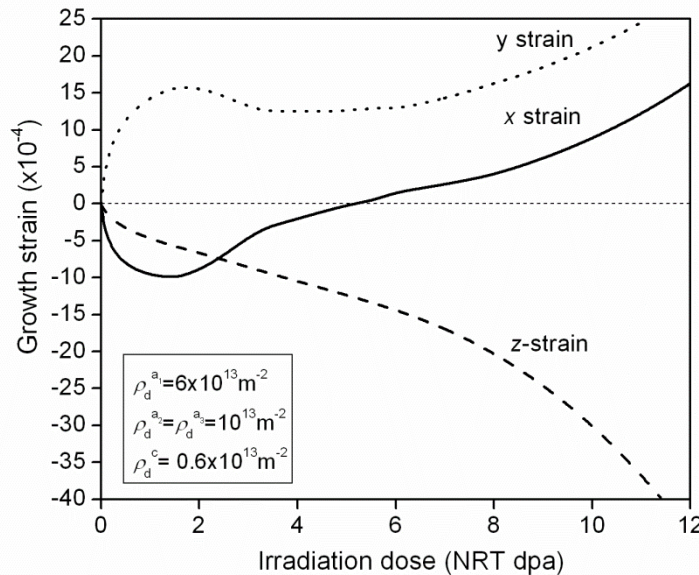
$$\frac{\dot{\rho}_{a_1}}{\dot{\rho}_{a_2}} = \frac{2N_v^{a_1}\rho_{a_2}}{N_i^{a_2}\rho_{a_1}} \left[ 1 - \frac{3\rho_c}{2(\rho_{a_1} - \rho_{a_2}) + \rho_c} \right] < 1. \quad (34)$$

This scenario is demonstrated in Figures 12 and 13, which were calculated for the same scenario of vacancy and interstitial prismatic loop nucleation, when  $N_v^{a_1} = N_i^{a_2}$ , and for  $\rho_d^{a_1} = 6\rho_d^{a_2}$  (see inset in Figure 13). The vacancy loops in the  $\mathbf{a}_1$  direction and interstitial loops in  $\mathbf{a}_2$  and  $\mathbf{a}_3$  directions grow very fast for a short period. Then, vacancy loops start to dissolve, and interstitial loops start to grow in the  $\mathbf{a}_1$  direction. Vacancy loops in the  $\mathbf{a}_2$  and  $\mathbf{a}_3$  directions temporarily grow then shrink during a transition period, when vacancy loops shrink in the  $\mathbf{a}_1$  direction. Then interstitial-type loops grow in all three  $a$  directions.

Figure 13 shows that for the case considered, the strain in the direction where vacancy loops grow is negative for about six dpa. Then, after vacancy loops dissolve, the strain becomes positive and increases similarly to those in other two directions. This picture is similar to that observed experimentally [17]. At higher irradiation doses the  $x$  and  $y$  strains approach each other as shown in the black dotted and dashed lines in Figure 14.



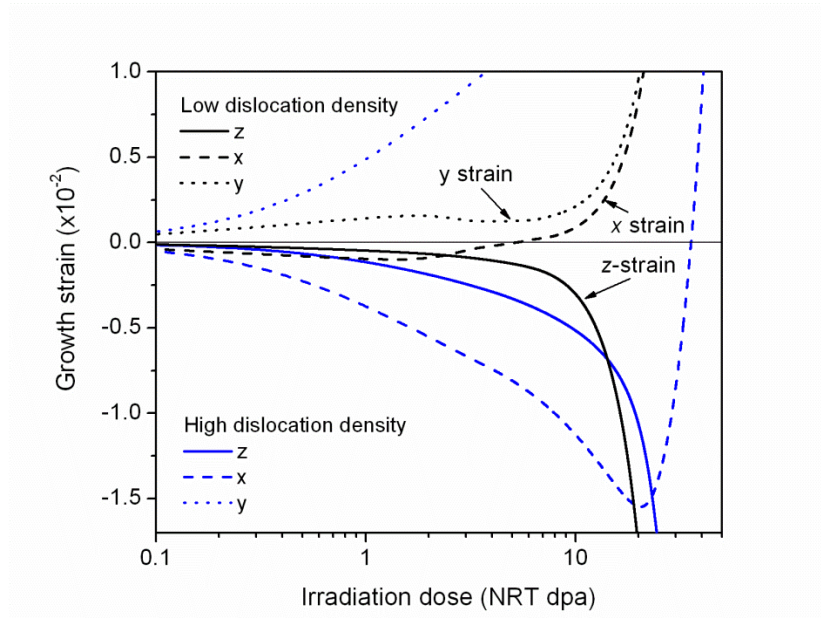
**Figure 12.** Dose dependence of sessile interstitial and vacancy loop radii calculated for the case in which the initial density of  $a_1$  dislocations is six times higher than in the other two directions.



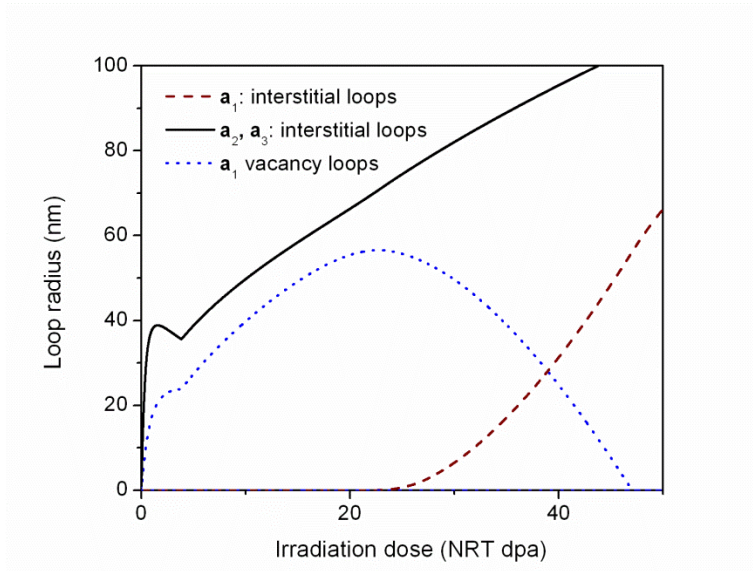
**Figure 13.** Dose dependence of growth strain for the case in which the initial density of  $a_1$  dislocations is six times higher than in the other two directions.

Figure 14 shows the dose dependence of the growth strain for the same case as in Figure 13, designated as low dislocation density, and for the case when all dislocation densities are increased by an order of magnitude, designated as high dislocation density. The corresponding changes of the loop radii are shown in Figure 15. For the higher dislocation density, vacancy loops grow over a longer dose range but the accumulation of loops eventually breaks the inequality of Eq. (33). Then, the  $x$  strain changes its sign and approaches the asymptotic behavior of the  $y$  strain. Thus, the observed negative  $a$ -strains, which were discussed extensively in the

literature [16], are clearly explained by the present calculations. Moreover, it is shown that the negative strains are expected to exist only in a certain dose range and disappear at high enough doses.



**Figure 14.** Dose dependence of growth strain for the same case as in Figure 13 designated as low dislocation density, and for the case in which all dislocation densities are increased by an order of magnitude.



**Figure 15.** Dose dependence of loop radii for the same case as in Figure 14.

In the calculations discussed above, vacancy loops grow in one and interstitial loops in the other two  $a$  directions, which is due to a corresponding distribution of initial dislocation densities in these direction. The situation is obviously symmetric; vacancy loops may grow in two directions and interstitial loops in one direction if the dislocation densities in two  $a$  directions are higher. This is demonstrated in Figures 16 and 17 for the loop strains and radii, respectively. The

description of the figures is the same as for Figures 14 and 15, and a scenario in which vacancy loops initially grow but then dissolve is realized in this case as well.

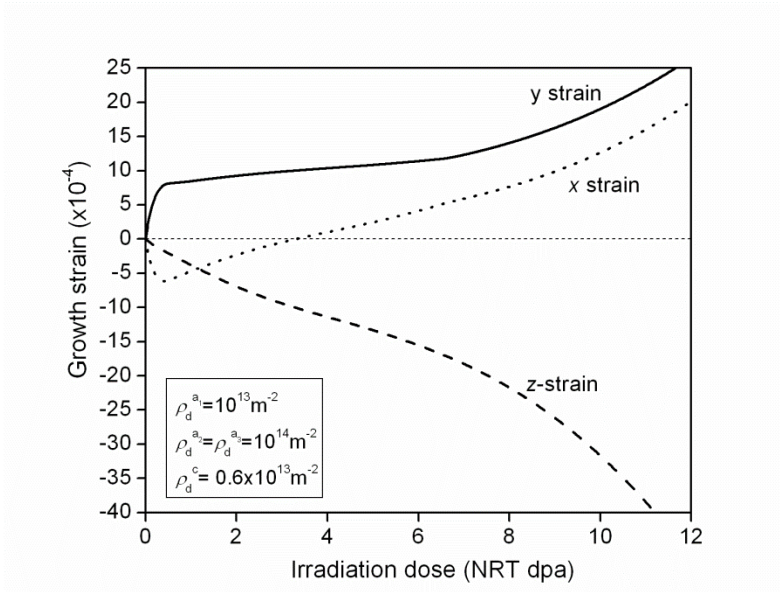


**Figure 16.** Dose dependence of growth strain for the case in which the initial density of  $a_1$  dislocations is ten times lower than in the other two  $a$  directions.

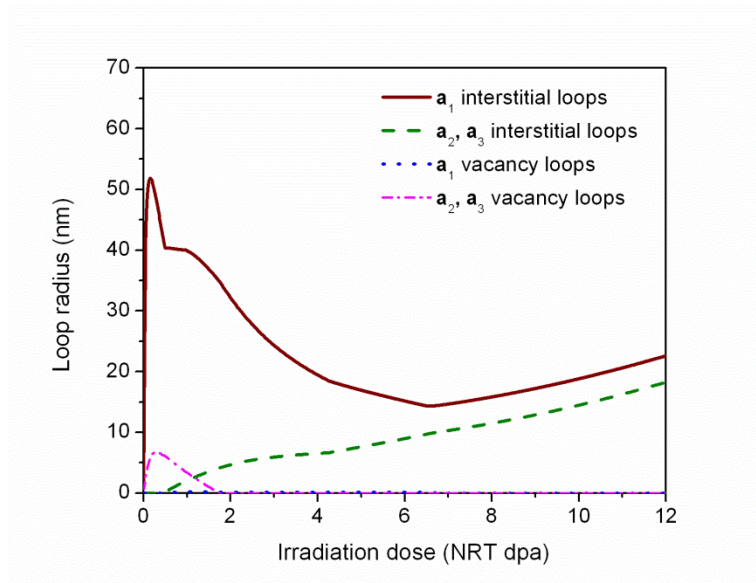


**Figure 17.** Dose dependence of loop radii for the same case as in Figure 16.

### 3.5. The maximum strain rate

In the previous section, the assumption that  $N_v^{a_1} = N_i^{a_2}$  was used and vacancy loops eventually dissolve in all the cases considered,. This is because interstitial loops grow faster, i.e. their line density increases more rapidly, than do the vacancy loops, and as a consequence the condition of Eq. (33) was eventually broken. The maximum strain rate is then limited by Eq. (29). This equation gives the maximum  $a$ -strain rate of  $\sim 0.16\%/dpa$ , which is an order of magnitude smaller than the maximum value possible in the proposed model, which is about  $1\%/dpa$  for  $\chi = 0.02$ . It is interesting that such high rates have observed in Zr-Pu alloys [18].

To obtain high strain rates, which are close to theoretical maximum of our model, i.e.  $\sim 1\%/dpa$ , one should assume that vacancy loops nucleate faster than interstitial loops, so that vacancy loop

line density increases faster than interstitial loop line density, i.e.  $\frac{\dot{\rho}_{a_1}}{\dot{\rho}_{a_2}} \approx \frac{2N_v^{a_1}\rho_{a_2}}{N_i^{a_2}\rho_{a_1}} > 1$ . Figure 18

shows the growth strain behavior for different maximum concentrations of  $a$ -type vacancy loops in one of the  $a$  directions. The black solid line shows the basic case, which is same as that shown in Figure 8, for which  $x$  and  $y$  strains are both positive at high irradiation doses and the maximum strain reached at 100 dpa is  $\sim 16\%$ . For 10 and 100 times higher maximum values of the vacancy loop number density, the  $x$  ( $\mathbf{a}_1$  direction) strain always remains negative, the  $z$  strain close to zero, and the  $y$  strain is positive and close to the absolute value of the  $x$  strain. For the highest number density, the  $y$  strain reaches  $\sim 80\%$  and the  $x$  strain reaches the same negative value, which is close to theoretical maximum. Thus, maximum  $a$ -strain rates of the order of  $1\%/dpa$  may take place if one  $a$  direction expands due to accumulation of  $a$ -type interstitial loops and the other contracts due to  $a$ -type vacancy loops, with relatively small changes in  $c$  direction.

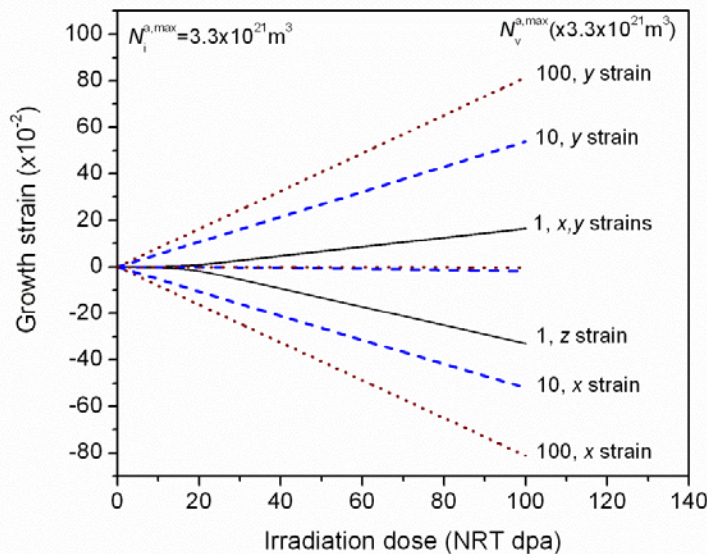


**Figure 18.** Growth strain behavior for different maximum concentrations of  $a$ -type vacancy loops in one of the  $a$  directions. The numbers 10 and 100 show the ratio of  $N_v^{a_1} / N_i^{a_2}$ . Note that  $c$  strains in both the cases are close to zero.

### 3.6. Dislocation climb velocities

Figures 19 and 20 show dose dependence of dislocation climb velocities. As can be seen, *c* dislocations climb faster than *a* dislocations because of their relatively lower line density. They climb only by capturing an excess of vacancies and their rate decreases steadily due to constant accumulation of the total sink strength in the form of dislocation loops.

In contrast, *a* dislocations climb slower than *c*-dislocations due to higher dislocation density, and their dose dependence is more complicated. They capture both PDs and SIA clusters, and their climb rate increases at doses  $\sim 3$ -6 dpa due to nucleation and growth of vacancy *c*-loops, which capture vacancies. At higher doses, the velocity starts decreasing again, as seen on figure 20.

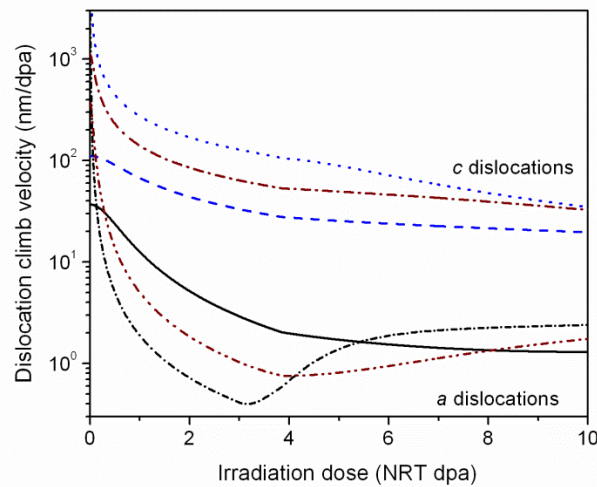


**Figure 19.** Dislocation climb velocities at small irradiation doses for *c* dislocations (dotted, blue –dislocation density  $10^{12} \text{ m}^{-2}$ ; dash dot, wine -  $10^{13}$ ; dash, blue -  $10^{14}$ ) and *a* dislocations (dot dash dot, black -  $10^{12}$ ; dash dot dot, wine -  $10^{13}$ ; solid, black -  $10^{14}$ ).

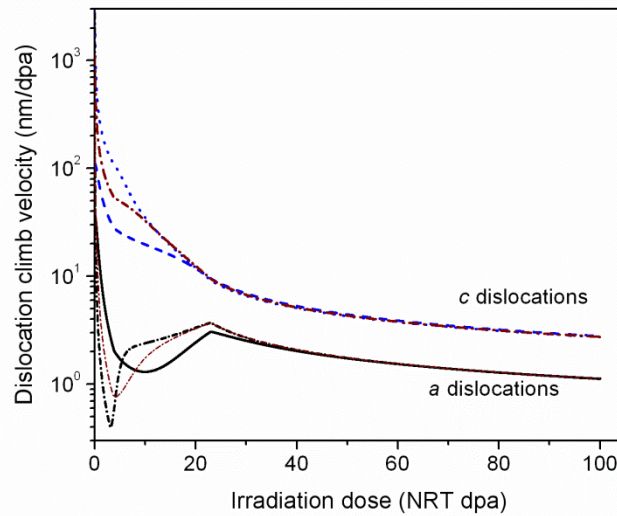


**Figure 20.** Dislocation climb velocities as in Figure 19 but for a wider dose range.

## 4. SUMMARY

1. The computer code RIMD-ZR.V1 (**Radiation Induced Microstructure and Deformation of Zr, Version 1**) which implements the model of radiation growth of Zr proposed recently in Ref. [1] has been presented. The mean-size approximation for the description of sessile vacancy and interstitial loops was employed, which is capable of describing the main features of microstructural evolution in Zr.
2. The basic parameters of the model have been fitted to the experimental data available. The values are:  $\varepsilon_r=0.9$ ,  $\varepsilon_i^g=0.2$ , with the number density functions described in Section 2.5 (the reaction radii  $r_{cd} = r_{cvi} = r_{cil} = 0.6$  nm were used). The cascade damage production parameters,  $\varepsilon_r, \varepsilon_i^g$ , are the same as those extracted from swelling experiments on fcc copper [7] and required to reproduce steady-state swelling rates observed in austenitic stainless steels at high irradiation doses [10].
3. The calculations reproduce all the stages observed in the dose dependence of RG strain, including ‘break-away’ growth of pre-annealed materials, and account for such striking observations as negative strains in the prismatic directions and the co-existence of vacancy- and interstitial-type prismatic loops.
4. The strain rate at high enough doses is found to be determined by the ratio of maximum number densities of interstitial prismatic and vacancy basal loops, see Eq. (29). One way to improve the radiation resistance of Zr may therefore be to suppress *c*-type loop nucleation.
5. The calculations confirm the maximum *a*-strain rate of  $\sim \chi / 2 \approx 1\%$  / dpa predicted by the model [1]. Such a large strain is observed in Zr-Pu alloys [18]. This may occur if the dislocation distribution in prismatic directions of the sample is highly anisotropic and some specific aspects of loop nucleation are satisfied. It requires that the vacancy and interstitial prismatic loops coexist in a wide dose range, so that crystal expands in one *a* direction and contracts in the others, while the *c* strain is much smaller.
6. The computer code provides the climb velocities for dislocations of different Burgers vector orientation, which are required for calculating creep rates using the climb-induced glide models. Thus, the model provides a necessary link to the description of creep.

The calculations have revealed a crucial dependence of the strains on the loop number densities, especially in the high dose limit, see Eq. (30). Thus, further progress in this area is only possible if the physical mechanisms of sessile loop nucleation are elucidated.

Finally, we would like to emphasize that the predicted maximum value of the RG strain rate for Zr of  $\sim 1\%$ /dpa is the same as the maximum swelling rate found for cubic materials (see discussion in Ref. [10]). Such a similarity appears to reflect a fundamental aspect of cascade-induced radiation damage in the bcc, fcc and hcp metallic crystals, and is a strong indication that the Production Bias Model [12], which was originally developed for cubic materials, provides a unified framework for the theory of radiation damage.

## REFERENCES

- [1] S.I. Golubov, A.V. Barashev, R.E. Stoller, ORNL Report: ORNL/TM-2011/473, (2011).
- [2] S.N. Buckley, Properties of Reactor Materials and Effects of Radiation Damage, ed. W.J. Littler (Butterworths, London, 1962) p. 413.
- [3] R.A. Holt, J. Nucl. Mater. **372** (2008) 182.
- [4] S.J. Wooding, L.M. Howe, F. Gao, A.F. Calder, D.J. Bacon, J. Nucl. Mater. **254** (1998) 191.
- [5] R. E. Stoller, "Primary Radiation Damage Formation," in Comprehensive Nuclear Materials, R. J. M. Konings, T. R. Allen, R. E. Stoller, and S. Yamanaka, Editors, Elsevier Ltd., Amsterdam, 2012, pp. 293-332..
- [6] R.A. Holt, C. H. Woo, C.K. Chow, J. Nucl. Mater. **205** (1993) 293.
- [7] S.I. Golubov, B.N. Singh, H. Trinkaus, Phil. Mag. A **81** (2001) 2533.
- [8] G.P. Walters, J. Nucl. Mater. **136** (1985) 263.
- [9] W.G. Wolfer, Computer-Aided Mater. Des. **14** (2007) 403.
- [10] A.V. Barashev, S.I. Golubov, Phil. Mag. **89** (2009) 2833.
- [11] B.N. Singh, S.I. Golubov, H. Trinkaus, A. Serra, Yu.N. Osetsky, A.V. Barashev, J. Nucl. Mater. **251** (1997) 107.
- [12] S.I. Golubov, A.V. Barashev, R.E. Stoller, "Mean Field Reaction Rate Theory", In: Encyclopedia of Comprehensive Nuclear Materials, Chapter 29, edited by Rudy Konings, Elsevier Ltd. (2011).
- [13] Y. de Carlan, C. Regnard, M. Griffiths, D. Gilbon, C. Lemaignan, ASTM STP **1295** (1996) 638.
- [14] A.V. Barashev, S.I. Golubov, H. Trinkaus, Phil. Mag. A **81** (2001) 2515.
- [15] S.I. Golubov, A.M. Ovcharenko, A.V. Barashev, B.N. Singh, Phil. Mag. A **81** (2001) 643.
- [16] L.D. Landau, E.M. Lifshitz, Theory of Elasticity, 3<sup>rd</sup> Edition, (Course of theoretical physics, vol. 7), Elsevier, 1986.
- [17] G.J.C. Carpenter, R.H. Zee, A. Rogerson, J.F. Watters, J. Nucl. Mater. **159** (1988) 86.
- [18] J.A. Horak, H.V. Rhude, J. Nucl. Mater. **3** (1961) 111.

## APPENDIX A. COMPUTER CODE RIMD-ZR.V1

A computer code named RIMD-ZR.V1 (Radiation Induced Microstructure and Deformation of Zr) realizing the diffusion-reaction model described in the above sections has been developed and written on FORTRAN 95 (see AI.4.2). It calculates evolution of the microstructure of irradiated sample: the loop mean sizes and number densities, accumulated strains and dislocation climb rates for different directions as functions of irradiation dose.

SI units are used throughout the code: [NRT dpa] for irradiation dose, [m] for loop radii, [m<sup>-2</sup>] for line densities, [m<sup>-3</sup>] for number densities, [m/s] for velocities.

When incorporating the code into larger-scale simulations, it is important to know the corresponding computational cost. On 2 GHz Intel processor, the speed of our calculations was estimated to be  $\sim 6 \times 10^{-7}$  s/dose step.

### A1. Structure of the code

Calculations start with reading input parameters from a separate file ‘RIMD-ZR.v1.dat’ (see AI.4.1). This file contains input values (see A1.2, Table A1) for the initial state of the sample, irradiations conditions, reaction-diffusion scenario and the parameters defining integration and output. In addition, it contains a short description of input parameters and description of main output files.

The initial state of a sample is characterized by edge dislocation densities for all four independent crystallographic directions, with the corresponding Burgers vectors  $b_j$ .

The irradiation conditions are defined by the NRT standard rate  $G^{\text{NRT}}$ , the fractions of the defects surviving recombination in cascades  $1 - \varepsilon_r$ , and forming glissile clusters,  $\varepsilon_i^g$ .

The calculations start with setting the initial state of the sample, which is setting to zero strains, the loop sink strengths, calculating sink strengths of dislocations for glissile SIA clusters. In the calculations of the vacancy and interstitial loops we used initial condition  $S_{i,v}^m = S_0$ , where  $S_0$  is equal to some small value,  $\sim 10^{-10}$ . The calculations were insensitive to this number.

Then, defect production rates and fluxes in all four crystallographic directions are calculated according to Eqs. (12)-(14). Eqs. (6), **Error! Reference source not found.**, (19) and (20) are used for the total dislocation densities and sink strength for 1-D diffusing SIA clusters. Note that the concentrations of mobile defects enter the analysis only as the products with the diffusion coefficients (i.e. as defects fluxes), hence the absence of the diffusion coefficients in the list of input parameters. If the diffusion coefficients are introduced, the concentrations will readily be obtained. Here, we did not need such calculations.

Then, the total numbers of defects accumulated in the loops of different types is updated using Eqs. (16)-(18), with the sink strength defined by Eqs. (19) and (20). As a next step, the code updates the number densities of the defects clusters Eqs. (27) and (28). Using knowledge on the

total number of defects accumulated in the loops of any particular type and the number density of the same loops, Eq. (15) is used to calculate the mean radius of the loops, which represents the mean-size approach.

The accumulated strains are calculated according to Eqs. (21)-(23) and the velocities of dislocations with the Burgers vectors along particular directions from Eq. (26). In addition, the strains in the Cartesian coordinate system with the  $x$  axis along  $\mathbf{a}_1$  direction, i.e. for  $\alpha=0$ , are calculated using Eq. (23). In the same coordinate system, the velocities of dislocations along coordinate axes are calculated as if they were real dislocations with the Burgers vectors along corresponding axes.

This finalizes calculation for one step of microstructure evolution, where new values for the number densities and radii of all type loops are now calculated.

The irradiation dose step for integration of differential equations is an external constant parameter to the code, and is normally chosen to be equal to  $\sim 10^{-4}$  NRT dpa, but two orders of magnitude higher value give similar results.

Table A2 (see section A3) describes the main output, which, of course, may be extended.

## A2. Input data to the code

**Table A1.** Input parameters to the code RIMD-ZR.V1.

Parameter	Name	Dimensions	Description
<b>Initial conditions</b>			
$\rho_d^{a_1}, \rho_d^{a_2}, \rho_d^{a_3}, \rho_d^c$	rhoda1, rhoda2, rhoda3, rhodc	$m^{-2}$	Densities of edge dislocations with Burgers vectors along $a_1, a_2, a_3$ and $c$ directions, respectively
$b_j$	bura, burc	m	Length of Burgers vectors of $a$ and $c$ dislocations
<b>Irradiation conditions</b>			
$G^{NRT}$	GNRT	NRT dpa/s	NRT standard dose rate
$1 - \varepsilon_r$	esurv	---	Defect survival fraction in displacement cascades
$\varepsilon_i^g$	eica	---	Fraction of SIAs produced in cascades in the form of interstitial glissile clusters
<b>Reactions and loop nucleation</b>			
$r_{cd}, r_{cvi}, r_{cil}$	rdcap, ricap, rvcap	m	Capture radii of dislocations and interstitial and vacancy loops for glissile SIA clusters
$\phi_v^{max}, \phi_i^{max}$	phiAI, phiAV	NRT dpa	Irradiation doses for the end of the nucleation stages of prismatic vacancy and interstitial loops (if continuous nucleation), respectively
$N_v^{m,max}, N_i^{m,max}$	dvlam, dilam	$m^{-3}$	Maximum values of the number density of vacancy and interstitial prismatic sessile loops
$\phi_{v0}^c$	phiC	NRT dpa	Irradiation dose from which vacancy $c$ -type loops start forming
$\Delta$	delta	NRT dpa	Irradiation dose for the end of the nucleation of sessile vacancy basal loops
$A$	AA	---	Parameter characterising nucleation of vacancy basal sessile loops, see Eq. (28)
$N_v^{c,max}$	dvlcm	$m^{-3}$	Maximum value of the number density of vacancy basal sessile loops
<b>Integration and output</b>			
$\phi^{max}$	phimax	NRT dpa	Maximum irradiation dose
$\Delta\phi$	dphi	NRT dpa	Irradiation dose integration step
$\Delta n$	nplot	---	Period for writing results in number of steps

Note that  $n_i^{ga}$  is not an input parameter: it is used, e.g. in Eq. (14), however only the total flux of glissile clusters  $n_i^{ga} D_{cl} C_{cl}^{m,ss}$  enters equations, see Eqs. (16)-(17).

### A3. Output files of the code

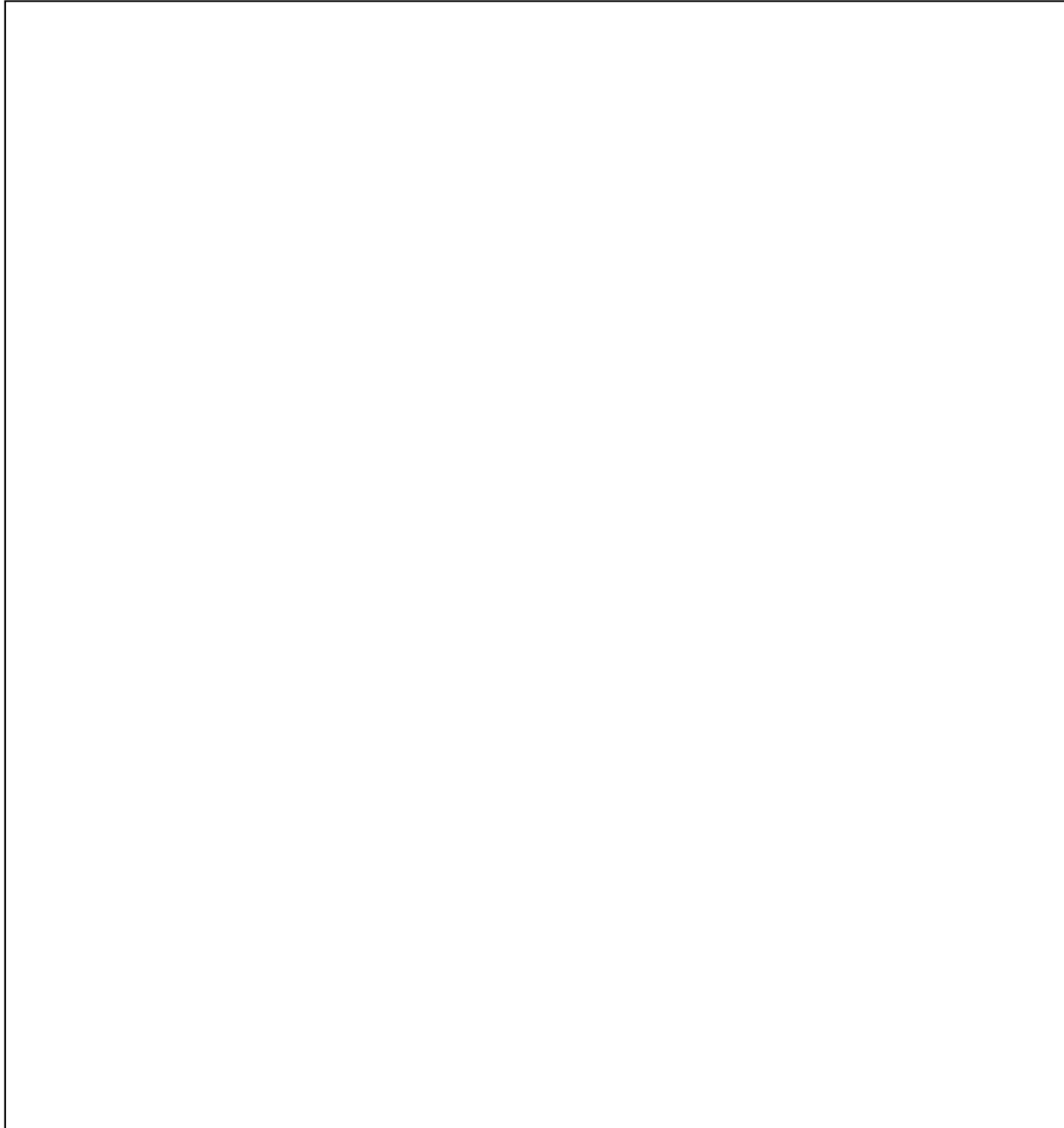
**Table A2.** Main output files of the code RIMD-ZR.V1.

N	Name	Output list	Paper notations	Description
10	Rimd-zr.txt	All input parameters	See Table 1	INPUT parameters in the sequence they were read
11	PartStr.txt	phiNRT, Epsc, Epsa1, Epsa2, Epsa3, SumEa	$\phi, \varepsilon_c, \varepsilon_{a_1}, \varepsilon_{a_2}, \varepsilon_{a_3},$ $\varepsilon_{a_1} + \varepsilon_{a_2} + \varepsilon_{a_3}$	Irradiation dose, $c$ and three $a$ strains, sum of all strains
12	V-dislc.txt	phiNRT, Vc, Va1, Va2, Va3	$\phi, V_c, V_{a_1}, V_{a_2}, V_{a_3}$	Dose, $c$ and 3 $a$ dislocation climb velocities
13	A1-axis.txt	phiNRT, rila1, densila1, rk2ila1, rvla1, densvla1, rk2vla1, rk2total	$\phi, r_i^{a_1}, N_i^{a_1}, k_{ia_1}^2,$ $r_v^{a_1}, N_v^{a_1}, k_{va_1}^2, \rho_{a_1}$	Dose, radius, number density and line density of interstitial and vacancy loops for $a_1$ direction, total dislocation density in this direction
14	A2-axis.txt	phiNRT, rila2, densila2, rk2ila2, rvla2, densvla2, rk2vla2, rk2total	$\phi, r_i^{a_2}, N_i^{a_2}, k_{ia_2}^2,$ $r_v^{a_2}, N_v^{a_2}, k_{va_2}^2, \rho_{a_2}$	Same for $a_2$ direction
15	A3-axis.txt	phiNRT, rila3, densila3, rk2ila3, rvla3, densvla3, rk2vla3, rk2total	$\phi, r_i^{a_3}, N_i^{a_3}, k_{ia_3}^2,$ $r_v^{a_3}, N_v^{a_3}, k_{va_3}^2, \rho_{a_3}$	Same for $a_3$ direction
16	C- axis.txt	phiNRT, rvlc, densvlc, rk2totc, ratc	$\phi, r_v^c, N_v^c, \rho_c, (\rho_c / \rho)$	Dose, radius and number density of vacancy loops for $c$ direction, total dislocation density in this direction and relative density
17	CXY-str.txt	phiNRT, Epsz, Epsax, Epsay, SumEx	$\phi, \varepsilon_z, \varepsilon_x, \varepsilon_y,$ $\varepsilon_x + \varepsilon_y + \varepsilon_z$	Dose, $c$ and $x$ and $y$ strains, sum of all strains ( $x=a_1$ )
18	V-dixyz.txt	phiNRT, Vz, Vx, Vy	$\phi, V_z, V_x, V_y$	Dose, dislocation velocities in $x, y$ and $z$ directions

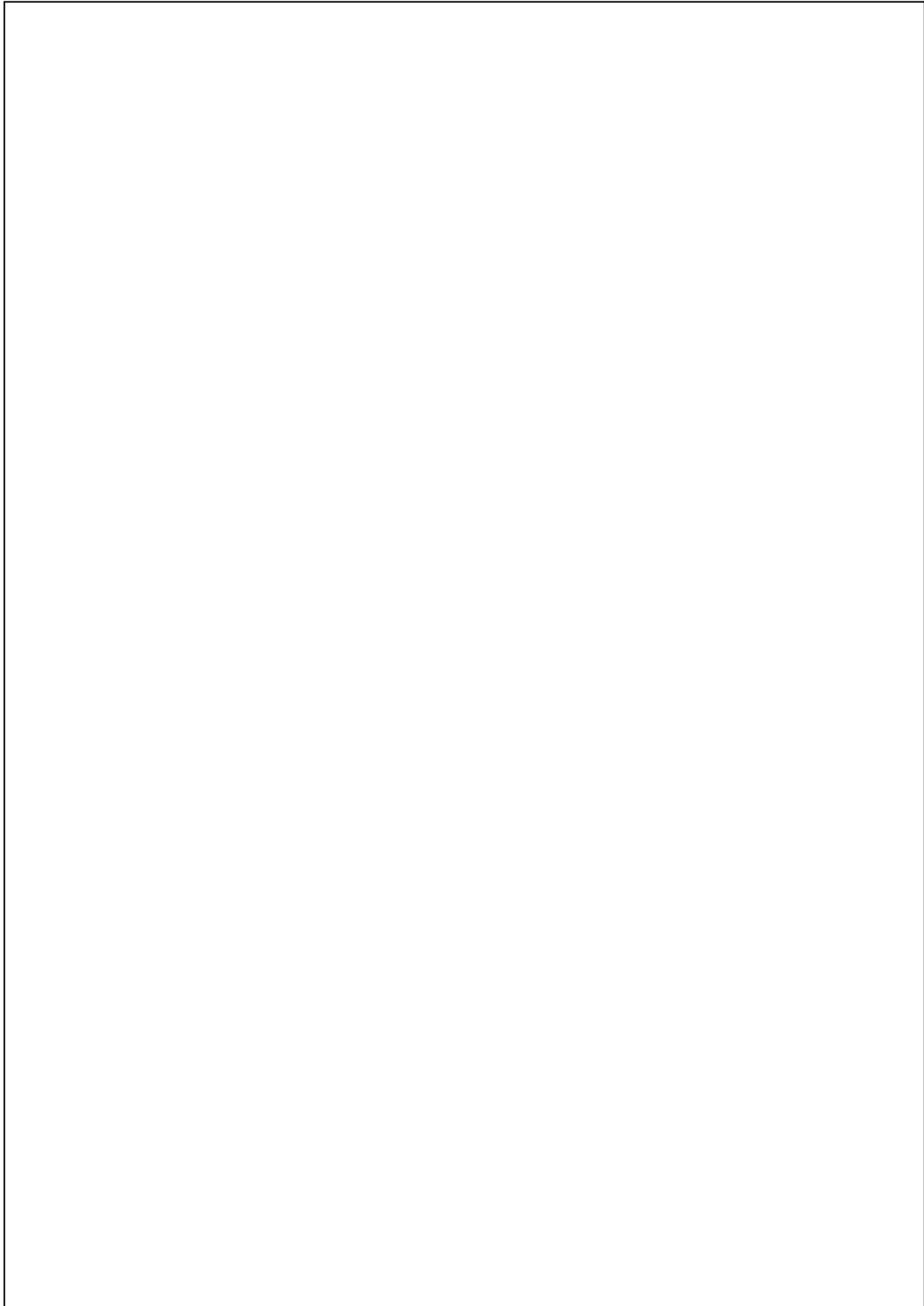
## A4. Source code

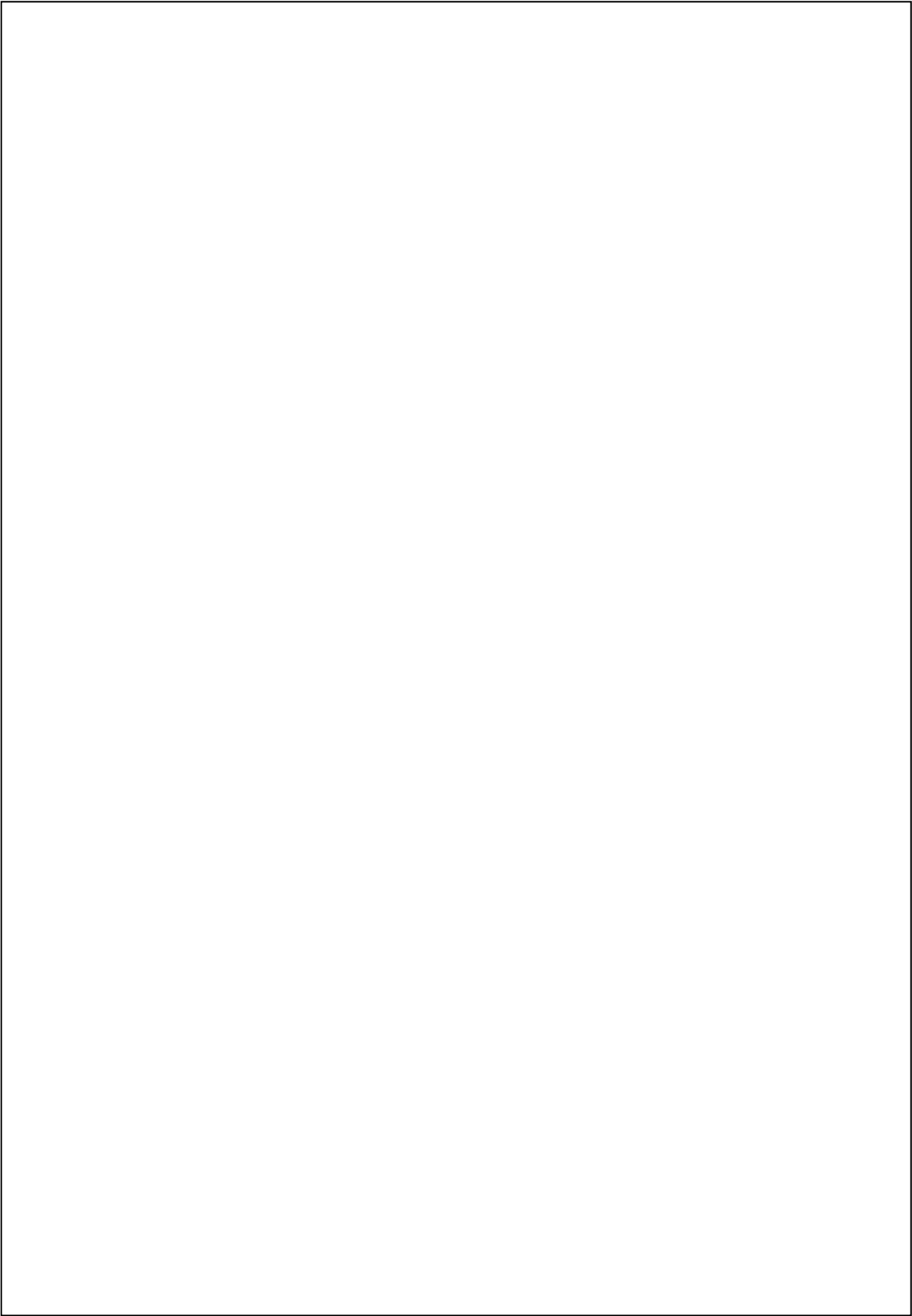
### A4.1. *Input file: RIMD-ZR.v1.dat*

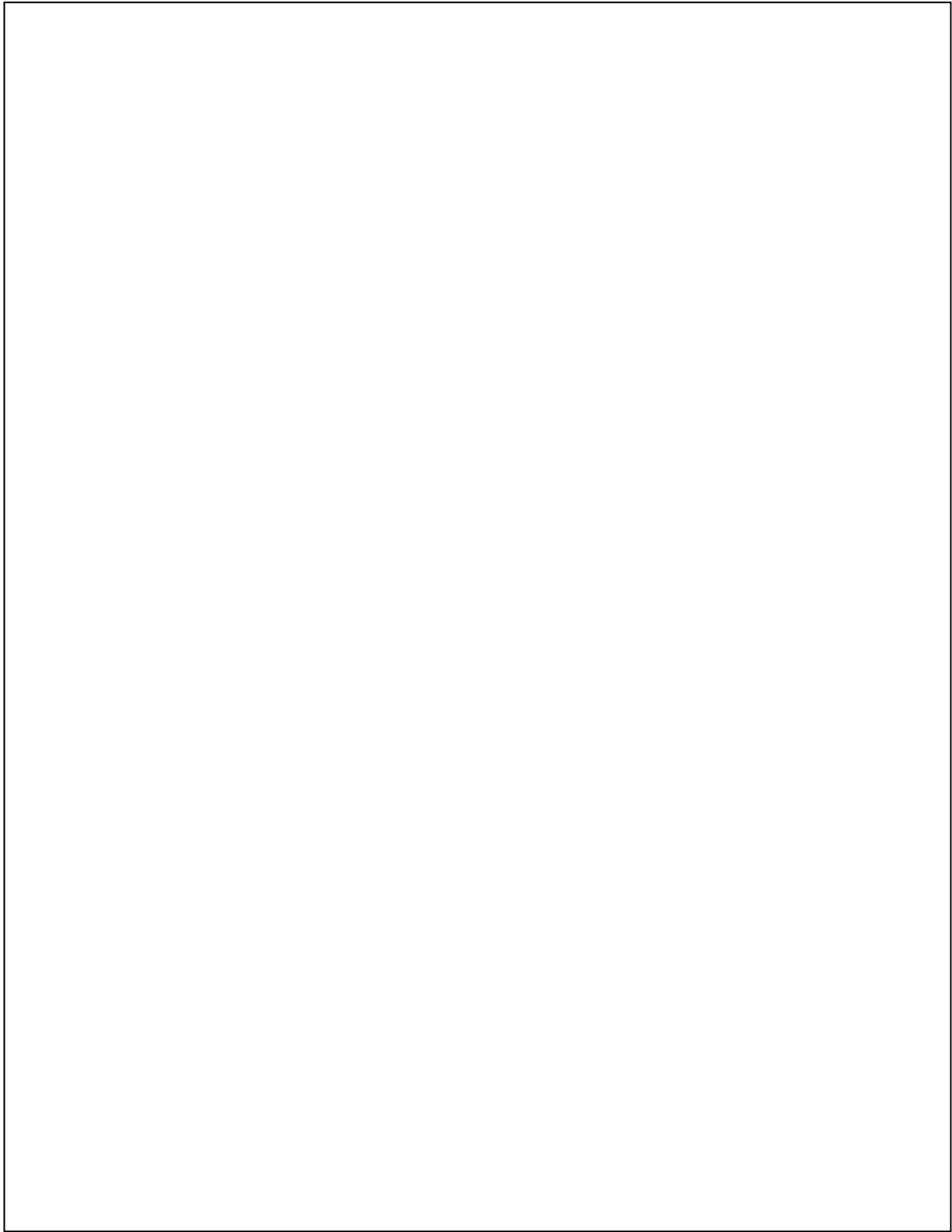
This is a format-free input.

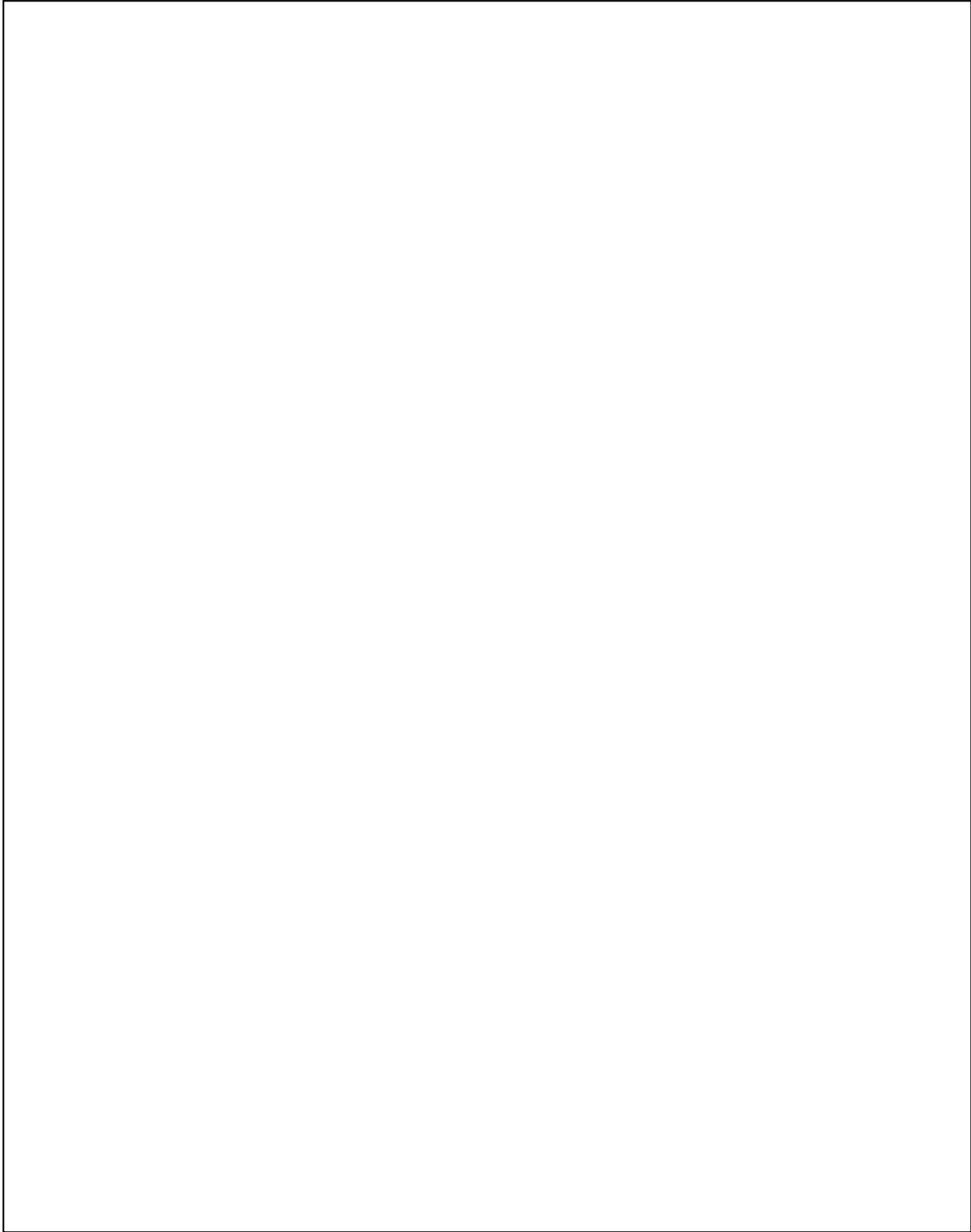


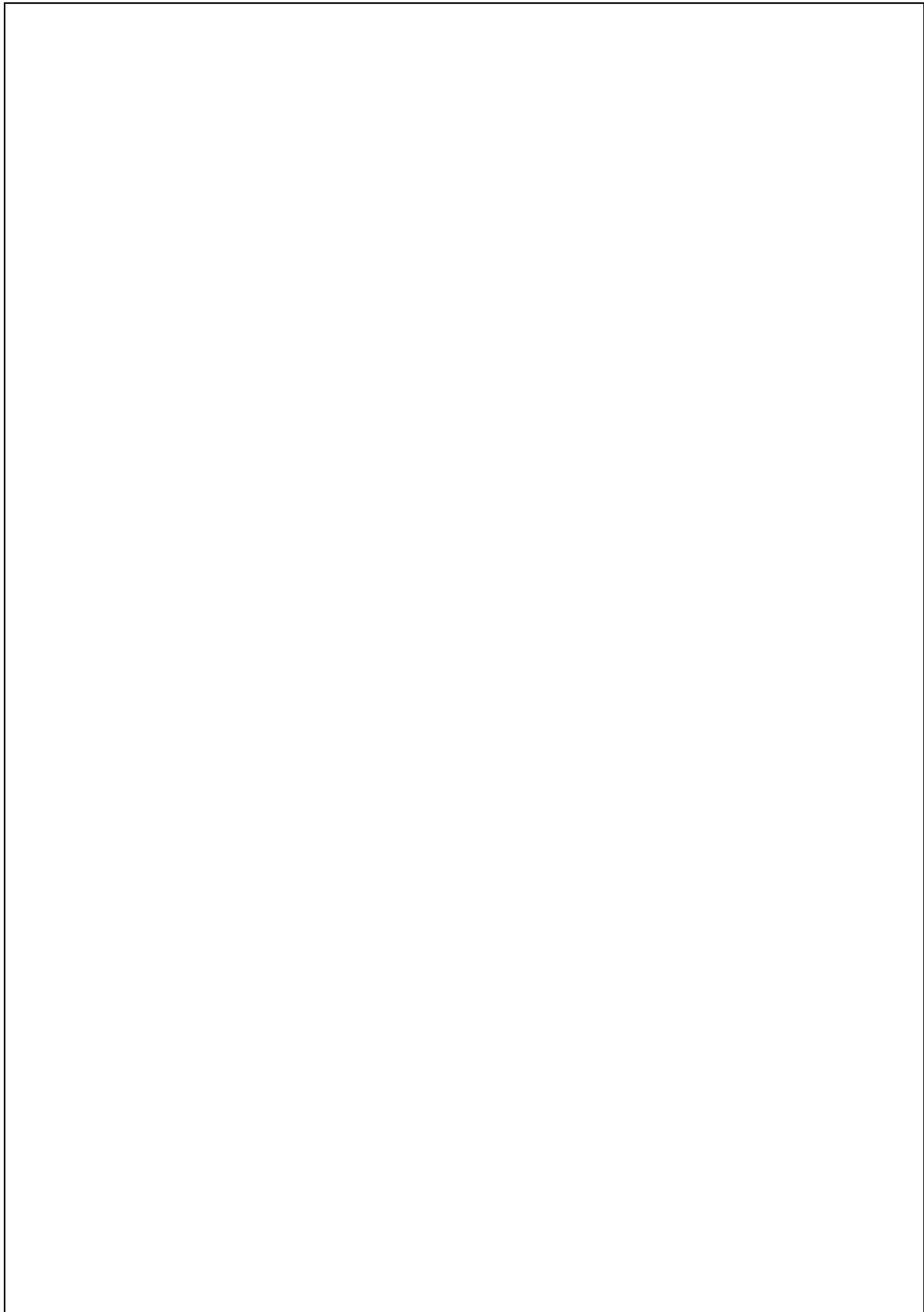
**A4.2. Main text: RIMD-ZR.f**

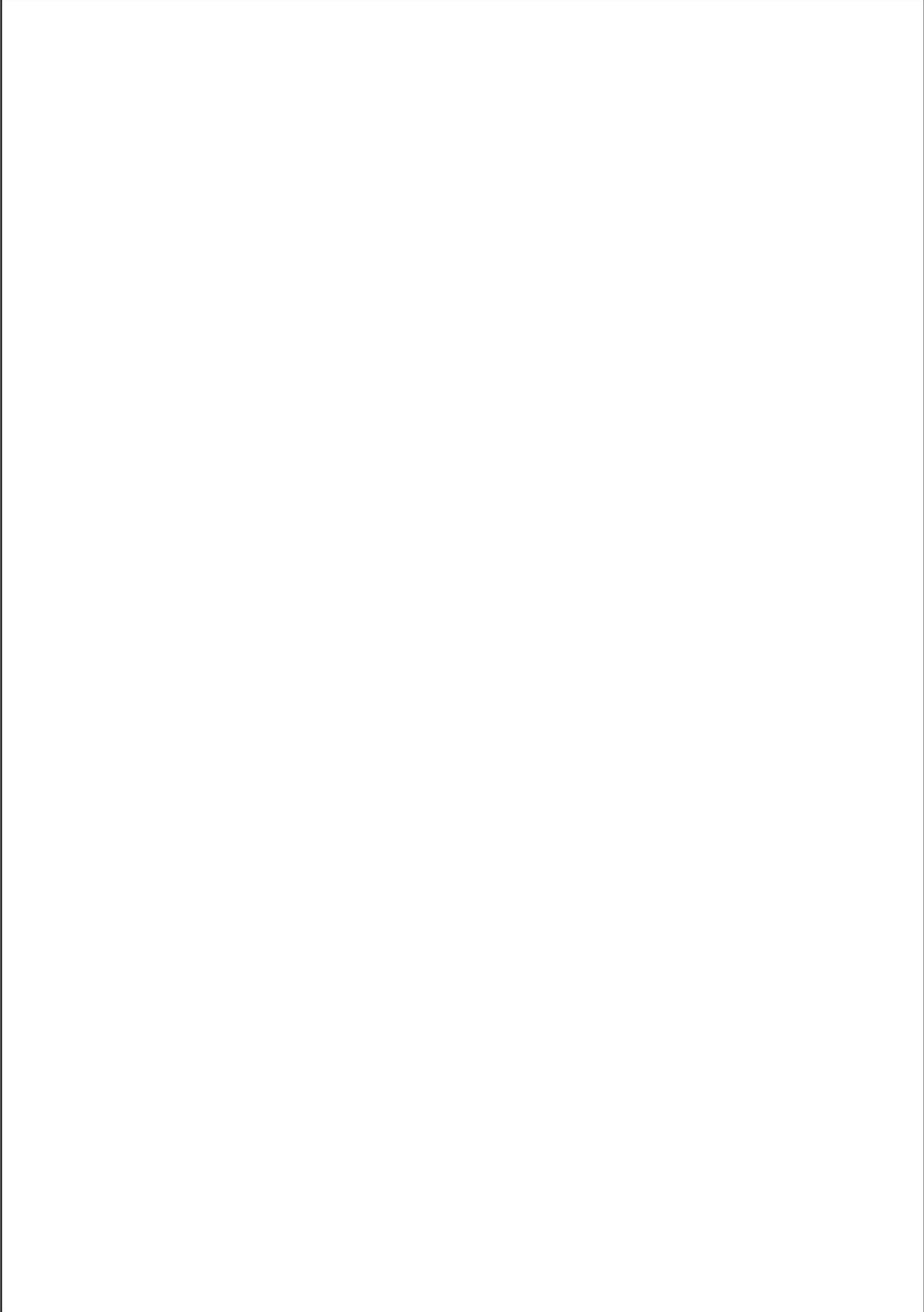














```
c
    close (10)
    close (11)
    close (12)
    close (13)
    close (14)
    close (15)
    close (16)
    close (17)
    close (18)
    close (19)
    close (20)

c
    stop
    end

c
c-----
c-----  END OF THE CODE  -----
c-----
```

**INTERNAL DISTRIBUTION**

1. A. V. Barashev, [barashevav@ornl.gov](mailto:barashevav@ornl.gov)
2. S. I. Golubov, [golubovsi@ornl.gov](mailto:golubovsi@ornl.gov)
3. G.I. Ice, [icege@ornl.gov](mailto:icege@ornl.gov)
4. D.B Kothe, [kothe@ornl.gov](mailto:kothe@ornl.gov)
5. J. R. Morris, [morrisj@ornl.gov](mailto:morrisj@ornl.gov)
6. D. N. Nicholson, [nicholsondm@ornl.gov](mailto:nicholsondm@ornl.gov)
7. Yu. N. Osetsky, [osetskiyyn@ornl.gov](mailto:osetskiyyn@ornl.gov)
  
8. M. Stocks, [stocksgm@ornl.gov](mailto:stocksgm@ornl.gov)
9. R. E. Stoller, [stollerre@ornl.gov](mailto:stollerre@ornl.gov)
10. B. Wirth, [wirthbd@ornl.gov](mailto:wirthbd@ornl.gov)
11. S. J. Zinkle, [zinklesj@ornl.gov](mailto:zinklesj@ornl.gov)
12. ORNL office of Technical Information

**EXTERNAL DISTRIBUTION**

1. C.A. English, Nexia Solutions, UK, [colin.a.english@nnl.co.uk](mailto:colin.a.english@nnl.co.uk)
2. D.J. Bacon, The University of Liverpool, Department of Engineering, Brownlow Hill, Liverpool, L69 3GH, UK, [djbacon@liverpool.ac.uk](mailto:djbacon@liverpool.ac.uk)
3. A. Serra, Universitat Politècnica de Catalunya, Dept. Matemàtica Aplicada III, ETSECCPB and CRNE, 08034, Barcelona, Spain, [a.serra@upc.edu](mailto:a.serra@upc.edu)
4. Malcolm Griffiths, Atomic Energy of Canada Limited, Chalk River Laboratories, Chalk River, Ontario, Canada, [griffithsm@aecl.ca](mailto:griffithsm@aecl.ca)
5. R.A. Holt, Department of Mechanical and Materials Engineering, Queen's University at Kingston, Ont., Canada K7L 1W9, [holt@me.queensu.ca](mailto:holt@me.queensu.ca)
6. V.N. Shishov, JSC VNIINM, Moscow, Russia Federation, [slava.shishov@bk.ru](mailto:slava.shishov@bk.ru)
7. Simon R. Phillpot, Department of Materials Science and Engineering, University of Florida, 100 Rhines Hall, PO Box 116400, Gainesville FL, 32611-6400, [sphil@mse.ufl.edu](mailto:sphil@mse.ufl.edu)
8. Donald R. Olander, Department of Nuclear Engineering, UC Berkeley, 4105 Etcheverry Hall MC 1730, Berkeley, CA 94720-1730, [fuelpr@nuc.berkeley.edu](mailto:fuelpr@nuc.berkeley.edu)
9. Arthur T. Motta, The Pennsylvania State University, 227 Reber Building, University Park, PA 16802, [atm2@psu.edu](mailto:atm2@psu.edu)
10. Donald Brenner, Department of Material Science and Engineering, North Carolina State University, Raleigh, NC, 276957907, [brenner@ncsu.edu](mailto:brenner@ncsu.edu)
11. Carlos N. Tome, MST-8, MS G755, Los Alamos National Laboratory, Los Alamos, New Mexico 87545, USA, [tome@lanl.gov](mailto:tome@lanl.gov)
12. B.P. Uberuaga, Materials Science and Technology Division, Los Alamos National Laboratory, Los Alamos, New Mexico 87545, USA, [blas@lanl.gov](mailto:blas@lanl.gov)

13. C. Domain, EDF-R&D Department MMC, Les Renardieres, F-77818 Moret sur Loint Cedex, France, [christophe.domain@edf.fr](mailto:christophe.domain@edf.fr)
14. F. Willaime, Service de Recherches de Metallurgie Physique, DMN-SRMP, CEA Saclay, 91191 Gif-sur-Yvette, France, [francois.willaime@cea.fr](mailto:francois.willaime@cea.fr)
15. Ishino Shiori, Editor of Journal of Nuclear Materials, [ishino@k9.dion.ne.jp](mailto:ishino@k9.dion.ne.jp)
16. H. Kaburaki, Nuclear Science and Engineering Directorate: Japan Atomic Energy Agency, Japan, [kaburaki.hideo@jaea.go.jp](mailto:kaburaki.hideo@jaea.go.jp)
17. Robert Comstock, Westinghouse Electric Co., Research & Technology, Pittsburgh, PA, USA, [comstorj@westinghouse.com](mailto:comstorj@westinghouse.com)
18. S.L. Dudarev, EURATOM/UKAEA Fusion Association, Culham Science Centre, Oxfordshire OX14 3DB, UK, [Sergei.Dudarev@UKAEA.org.uk](mailto:Sergei.Dudarev@UKAEA.org.uk)
19. A. Legris, Bâtiment C6 – 225, Unité Matériaux et Transformations, Bât. C6, Université Lille1, 59655 Villeneuve d'Ascq, France, [alexandre.legris@univ-lille1.fr](mailto:alexandre.legris@univ-lille1.fr),
20. D. Nguyen-Manh, Materials Modeling Laboratory, Department of Materials, University of Oxford, Parks Road, Oxford OX1 3PH, [manh.nguyen@materials.ox.ac.uk](mailto:manh.nguyen@materials.ox.ac.uk)
21. M.W. Finnis, Imperial College London, Department of Materials, 105 Royal School of Mines, South Kensington Campus, [m.finnis@imperial.ac.uk](mailto:m.finnis@imperial.ac.uk)
22. A. Sutton, Imperial College London, Department of Materials, 105 Royal School of Mines, South Kensington Campus, [a.sutton@imperial.ac.uk](mailto:a.sutton@imperial.ac.uk)
23. F. Soisson, Service de Recherches de Metallurgie Physique, DMN-SRMP, CEA Saclay, 91191 Gif-sur-Yvette, France, [Frederic.soisson@cea.fr](mailto:Frederic.soisson@cea.fr)
24. Sidney Yip, Department of Nuclear Science and Engineering, Massachusetts Institute of Technology, 77 Massachusetts Avenue, 24-107, Cambridge, MA 02139, [syip@MIT.EDU](mailto:syip@MIT.EDU)
25. C.R Stanek, Los Alamos National Laboratory, Los Alamos, New Mexico 87545, USA, [stanek@lanl.gov](mailto:stanek@lanl.gov)
26. G.S. Was, University of Michigan, Nuclear Engineering and Radiological Sciences, Cooley Building, Ann Arbor, MI 48109-2104, USA, [gsw@umich.Edu](mailto:gsw@umich.Edu)
27. M.I. Mendeleev, Materials and Engineering Physics, Ames Laboratory, US DOE, 207 Metals Development, Ames, IA, USA, [mendeleev@ameslab.gov](mailto:mendeleev@ameslab.gov)
28. G.J. Ackland, 2502 JCMB, ICMCS School of Physics, University of Edinburgh, Edinburgh EH9 3JZ, G.J.[Ackland@ed.ac.uk](mailto:Ackland@ed.ac.uk)
29. D. Terentyev, Nuclear Materials Science, SCK-CEN, Boeretang 200, B-2400 Mol, Belgium, [dterenty@sckcen.be](mailto:dterenty@sckcen.be)
30. P. Vladimirov, Karlsruhe Institute of Technology (KIT), Institute for Applied Materials - Applied Materials Physics, Hermann-von-Helmholtz-Platz 1 IAM-AWP/MW, 76344 Eggenstein-Leopoldshafen, Germany, [Pavel.Vladimirov@kit.edu](mailto:Pavel.Vladimirov@kit.edu)